On the numerical inversion of the Laplace transform in the context of physical models with realistic damping

Sur l'inversion numérique de la transformée de Laplace dans le contexte de la modélisation physique avec amortissement réaliste

---

Karim Trabelsi
Denis Matignon
Thomas Hélie

2009D025

2009

Département Traitement du Signal et des Images
Groupe AAO : Audio, Acoustique et Ondes

Sur l'inversion numérique de la transformée de Laplace dans le contexte de la modélisation physique avec amortissement réaliste.

Karim TRABELSI*, Denis MATIGNON† et Thomas HÉLIE‡ ‡

Le présent document constitue le rapport de contrat avec l'ANR *Consonnes*, ANR-05-BLAN-0097-01, sur le thème général du *Contrôle des Sons Naturels et Synthétiques*.

Le travail a été réalisé par Karim Trabelsi lors d'un séjour post-doctoral entre le 1er Octobre 2006 et le 31 Août 2007 au sein du Laboratoire Traitement et Communication de l'Information, UMR 5141 du CNRS, sous la responsabilité de Denis Matignon, maître de conférences au département Traitement du Signal et des Images de Télécom ParisTech, avec la collaboration de Thomas Hélie, chargé de recherches au Laboratoire STMS de l'IRCAM, UMR 9912.

Ce document est dûment mentionné dans le rapport final de l'ANR *Consonnes*, en date du 28 Août 2009, au titre de la référence [27], page 9 ; rapport téléchargeable à l'adresse suivante :
`http://www.consonnes.cnrs-mrs.fr/consonnes-juillet2009_bibliographie_finale.pdf`

De plus, une première partie des résultats du travail de Karim Trabelsi avait fait l'objet d'une publication dans une conférence internationale, en juillet 2007 :

K. Trabelsi, Th. Hélie and D. Matignon. *Time-domain simulation of functions and dynamical systems of Bessel type.* In *Eight international conference on mathematical and numerical aspects of wave propagation phenomena*, pages 547–549. INRIA/SIAM, Reading (United Kingdom), july 2007.

*Karim Trabelsi, en séjour post-doctoral à Télécom-ParisTech, département TSI & CNRS, LTCI, 37-39, rue Dareau, 75014 Paris ; actuellement enseigant-chercheur à l'IPSA - LCSM, 5-9 rue Maurice Grandcoing, 94200 Ivry-sur-Seine, `karim.trabelsi@polytechnique.edu`

†Denis Matignon, maître de conférences à Télécom-ParisTech, département TSI & CNRS, LTCI, 37-39, rue Dareau, 75014 Paris ; actuellement professeur à l'ISAE, 10 avenue Edouard Belin, B.P. 54032 - 31055 Toulouse Cedex 4, `denis.matignon@isae.fr`

‡Thomas Hélie, chargé de recherche à l'IRCAM & CNRS, UMR 9912, 1, place Igor Stravinsky, 75004 Paris, `thomas.helie@ircam.fr`

On the numerical inversion of the Laplace Transform in the context of physical models with realistic damping

Th. Hélie, D. Matignon and K. Trabelsi

Résumé/Motivation

Ce rapport technique porte sur les recherches menées sous le thème *Optimisation numériques de modèles physiques avec amortissments réalistes pour la synthèse sonore en temps réel* et financées par le projet CONSONNES (CONtrôle de SONs instrumentaux Naturels Et Synthétiques). Le contexte de ce travail est la simulation en temps réel des résonateurs d'instruments à vent. Quelques modèles physiques réalistes comme, par exemple, l'équation des ondes avec pertes visco-thermiques dans un pavillon (modèle de The Webster-Lokshin, cf. [63]; voir aussi [45], [46] et [37]), exhibent des fonctions de tranfert non standard avec des poles, des points de branchement et des coupures dans les demi-plan gauche de Laplace, ce qui a pour effet, dans le domaine temporel, de produire des réponses impulsionnelles dites à mémoire longue dues à l'ammortissement non purement exponentiel. Une conséquence directe de ce phénomène est le besoin de simulation pour des temps longs. De plus, les réponses temporelles pour ce type de système s'obtiennent par inversion de la transformée de Laplace ce qui rajoute un deuxième problème numérique puisque l'exponentielle est très oscillante sur la droite de Bromwich.

Au fil des années, des méthodes ont été mises en place pour traiter le problème de l'inversion numérique de la transformée de Laplace. L'efficacité de la plupart d'entre elles dépend de certains paramètres qui sont réglés heuristiquement. De plus, beaucoup d'entre elles ne sont pas adaptées aux fonctions de Green non standard qui nous intéressent. A notre connaissance, les algorithmes les plus efficaces peuvent être classés selon quatre approches. La première est basée sur le développement en séries de Fourier. La seconde utilise des méthodes de collocation. La troisième est fondée sur une idée de Talbot [75] qui consiste à déformer le contour de Bromwich afin de faciliter l'intégration numérique. La dernière méthode, plus récente, vient de l'automatique et du contrôle, et consiste à approximer des représentations intégrales diffusives du système. Les deux dernières approches semblent plus efficaces et adaptées à nos besoins. Ainsi, nous avons suivi ces deux pistes avec pour but l'obtention de déformations optimales du contour de Bromwich afin d'implémenter des algorithmes qui sont au moins aussi performants que l'approche diffusive tout en ayant l'avantage d'être automatisés, évitant de la sorte tout réglage heuristique de paramètre.

Abstract/Motivation

This technical report sums up the research carried out under the title: *Numerical optimisation of physical models with realistic damping for real-time sound synthesis* which was supported by the CONSONNES (CONtrôle de SONs instrumentaux Naturels Et Synthétiques - in english: Control of natural and synthetic instrumental sounds) project. The context of this work is the real-time simulation of wind instrument resonators. Some realistic physical models as, for instance, the wave equation with viscothermal losses in a flared duct (The Webster-Lokshin model, cf. [63]; see also [45], [46] and [37]), possess non standard Green (transfer) functions with poles, branchpoints and cuts in Laplace's left halfplane, which entails, in the time domain, impulse responses that

decay slowly due to the non-purely-exponential damping. This accounts for the the *long memory* label tagged to such a model. A straightforward consequence to this phenomenon is the need of simulation for long times. Moreover, the time responses to such systems are obtained through the inversion of the Laplace transform which adds a second numerical issue, since the exponential factor is highly oscillatory on the Bromwich line.

Over the years, methods have been devised to deal with the numerical inversion of the Laplace transform. The efficiency of most of these depends on some parameters that are tuned heuristically. Furthermore, most of them are not adapted to the nonstandard Green functions we are concerned with. To our knowledge, the most efficient algorithms may be divided along four directions. The first one is based on Fourier series expansion. The second one uses collocation methods. A third procedure is founded on Talbot's idea [75] which consists in deforming the Bromwich contour into a curve that allows for a better numerical integration. Last but not least is an approach that comes from automatic control and which consists in the approximation of diffusive integral representations of the system. The last two approaches seem more efficient and suitable for our purposes. Therefore, these were the tracks we investigated with the goal of obtaining optimal deformations of the Bromwich contour so as to work out algorithms that are at least as good as the diffusive approach with the advantage of being automatic, i.e., without parameters that have to be tuned or whatsovever.

Contents

1 How to numerically compute a function defined by a Bromwich integral?

One way of solving linear ordinary or partial differential equations is by computing its Green function, that is, the image of the solution in the Laplace domain, because it is easily obtained, then apply to it the inverse transform to determine the solution to the original equation. Fortunately, in some cases, the solution in the original time domain may be computed analytically, and such examples serve as test cases for numerical integration algorithms of this inversion which are necessary to the approximation of solutions for which no simple representation is known.

The inverse Laplace transform We recall the Laplace transform of a function $F : \mathbb{R}^+ \to \mathbb{C}$ defined in the time domain:

$$\widehat{F}(s) = \int_0^\infty \mathrm{e}^{-s\,t} F(t)\,\mathrm{d}t, \quad \Re s > -a_0, \tag{1}$$

where $\widehat{F}(s)$ is the image of the time domain solution, $F(t)$, to be inverted, and $-a_0$ is its convergence abscissa. In other words, the singularities of $\widehat{F}(s)$ lie in the halfplane $\Re s \leq -a_0$, and the function is analytical in the remaining halfplane. The above Laplace transform is inverted, at least theoratically, via the Bromwich formula:

$$F(t) = \frac{1}{2i\pi} \int_{a-i\infty}^{a+i\infty} \mathrm{e}^{s\,t} \widehat{F}(s)\,\mathrm{d}s, \quad a > -a_0, \tag{2}$$

where $s = a + \imath y$, $y \in \mathbb{R}$ is the Bromwich line. As already mentioned, the numerical approximation of the above integral is a tough challenge. Indeed, the exponential factor is highly oscillatory on the Bromwich line as the imaginary part tends to infinity. Moreover, the Green function $F(s)$ is nonstandard in the applications we are concerned with, as it has poles, branchpoints and cuts in the halfplane $\Re s \leq -a_0$. Finally, it can hardly pare down the oscillations, since it decays slowly as $|y| \to \infty$.

Nonstandard Green functions To illustrate what we mean by nonstandard Green functions, we shall give a concrete example of an equation we are keen on. It is a realistic physical model known as the Webster-Lokshin[1] model and describes the wave equation in a flared duct with visco-thermal losses:

$$(\partial_t^2 + \eta \partial_t^{\frac{3}{2}}) w - \frac{1}{r^2(z)} \partial_z [r^2(z) \partial_z w] = 0, \quad t > 0, \quad z \in]0, 1[.$$

to which we add dynamic impedance boundary conditions at $z = 0$, and observe at $z = 1$. This equation may be numerically dealt with in the Laplace domain through a conversion quadripoles formalism analogous to the waveguide decomposition reserved to the treatment of the wave equation; see [37]. Note that the equation above is nothing but a perturbation of the wave equation with small parameter $\eta > 0$. The scattering matrix associated with this equation consists of transmission and reflection functions that are made up of more or less singular transfer functions which we shall not explicit here; we refer the reader to Hélie & Matignon [37] for a full treatment of the issue. However, as a typical example of the Green functions we are concerned with, here is one such function:

$$\mathcal{H}_\eta(s) = \mathrm{e}^{-\Gamma_\eta(s)+s}, \quad \Gamma_\eta^2(s) = s^2 + \eta s^{\frac{3}{2}} + \Upsilon, \quad \eta > 0, \quad \Upsilon \in \{-1, 0, 1\},$$

[1] The name was given after the wave equation in a flared duct without loss due to Webster and the modeling of the viscothermal losses due to Lokshin [45, 46]; see also Polack [63]

where Υ depends on the curvature of the duct (1 for a flute, 0 for a trumpet, and -1 at the end of an English horn); for simulation, the duct is dissected into parts with almost constant curvature. The above function is analytic in $\mathbb{C}_0^+$, and its analytic continuation involves 3 branchpoints: 0 because of the term $s^{\frac{3}{2}}$ and the roots of $\Gamma_\eta^2(s)$. The associated cuts should be accordingly chosen in $\mathbb{C}_0^-$. We will see, in subsequent sections, how the choice of these cuts may influence the quality of the numerical integration by fixing the diffusive representation to be approximated, or by limiting the deformations of the Bromwich contours.

Long-time asymptotics Another important feature of the models we aim at simulating is their long-time asymptotics. Contrarily, to the solution of the wave equation without losses, for instance, where the response is periodic, we are concerned with realistically damped models, the solutions of which do not decrease exponentially in time in most cases. These will have an asymptotic behaviour that will be more like $\mathcal{O}\big(\frac{1}{t^\alpha}\big)$, $0 < \alpha < 1$, which clearly forbids short-time truncation, more so in a real-time simulation context. One of our reference test functions is, for instance, the first kind Bessel function of order 0 whose long-time asymptotic reads as follows:

$$J_0(t) \underset{\infty}{\approx} \sqrt{\frac{2}{\pi t}} \cos\Big(t - \frac{\pi}{4}\Big),$$

whose image in the frequency domain requires the definition of two cuts starting at $\pm\imath$:

$$\hat{J}_0(s) = \frac{1}{\sqrt{1+s^2}}.$$

In practice, long-time asymptotics are observed in many fields where damping such as hydrodynamics [27], seismology [29], acoustics [28, 55], and optics [10] to cite just a few. This is also a feature of models involving fractional derivatives to describe the damping in viscoelatic models as opposed to multi-modal Maxwell systems; see [42, 35, 54, 51, 52]; see also [81] for an application in rheological characterization. For an introduction to fractional calculus and related litterature, we send the reader to [53] and the references therein.

We would like to mention that in no way have we attempted to give, here, an exhaustive account on the history of the numerical inversion of the Laplace transform. We only hope to have given some guiding lines that may serve either as a teaser, or as a starting point for the interested reader. Note that an almost exhaustive list of references may be found here
`http://www.pe.tamu.edu/valko/public%5Fhtml/Nil/index.html`.

1.1 Optimizing parametrized Bromwich contours

This is not the first strategy devised in order to facilitate the numerical computation of the Bromwich integral. However, to this day, we may conjecture that this was the most brilliant intuition. Indeed, set off by the observation that the actual impediment to an accurate and efficient evaluation of the integral (2) are the high oscillations of the exponential term on the Bromwich line, Talbot [75] suggested that should the contour be deformed into a curve with real part tending to $-\infty$, the wishful outcome would be a fast decay of the integrand owing to the exponential term. Accordingly, this should allow a comfortable approximation of the integral by the trapezoidal rule. Now, Cauchy's theorem and Jordan's lemma (for instance, see [83]) ensure that, as long as singularities are not crossed during the deformation, this is possible if

1. $|\hat{F}(s)| \to 0$ uniformly as $|s| \to \infty$ with $\Re s \leq -a_0$. $(C1)$
2. $\exists K > 0$, such that for any singularity ξ of $\hat{F}$, we have $|\Im\xi| < K$. $(C2)$

And the general inversion formula would be

$$F(t) = \frac{1}{2i\pi} \int_{\mathbb{R}} \mathrm{e}^{\gamma(u)\, t} \widehat{F}(\gamma(u))\, \gamma'(u)\, \mathrm{d}u, \tag{3}$$

with $u \mapsto \gamma(u)$ a parametrization of the smooth curve $\Gamma = \gamma(\mathbb{R})$. Ultimately, once the rapid decay of integrand is achieved owing to the curve Γ, the numerical inversion of the integral should be easily manageable by the trapezoidal (or midpoint) rule. Thereby, the approximation may be expressed as follows:

$$F_{h,N}(t) = \frac{h}{2i\pi} \sum_{n=-N}^{N} \mathrm{e}^{\gamma(nh)t} \widehat{F}(\gamma(nh))\gamma'(nh). \tag{4}$$

where $N \in \mathbb{N}$ is the number of interpolation nodes (points where the integrand shall be evaluated), and $h > 0$ is the stepsize (space seperating consecutive nodes).

1.1.1 The Talbot contour

The Bromwich contour Talbot's original method was based on reads as:

$$\gamma(\theta) = \mu(\theta \cot\theta + \lambda i\theta) + \beta, \quad -\pi < \theta \leq \pi, \tag{5}$$

where μ and λ are positive reals, and β must satisfy $\beta + \mu > -a_0$. That said, in [62], it was remarked that the contour should move to the left without getting too close to the singularities, since $\left|\hat{F}(s)\right|$ would take large values at those nodes. Therefore, it would be more correct to impose

$$\beta + \mu > -a_0 + \epsilon, \tag{6}$$

where $\epsilon > 0$ is yet to be optimized/determined, since, to our knowledge, no work has adressed this issue be it for this contour or another. Note that [62] provides a `Fortran` implementation of the method as devised by Talbot. Numerical results are accordingly reported for Green functions displaying various kinds of singularities (essential singularities, branchpoints, cuts). They observe that essential singularities should stay at a certain "optimal distance" from the contour which is tuned experimentally. Moreover, they insist on the necessity of the first condition which, if not fulfilled by the transform, leads to unpredictable results especially for small times. We may conjecture that small times attenuate the fast decay of the exponential term induced by the contour, which combined with the proximity of the latter to the singularities neutralizes the design of the scheme. We shall discuss this issue later on; see paragraph 3.4.

More recently, Weideman [86] obtained almost optimal convergence rates for the Talbot contour (cotangent) by carefully choosing the parameters in order to optimize the convergence rate. Namely, he has improved the convergence rate from $\mathcal{O}(\mathrm{e}^{-c\sqrt{N}})$ to $\mathcal{O}(\mathrm{e}^{-c\,N})$, however the optimization is formal. Indeed, no proof of the optimality of the parameters is provided. In addition to that, the results are "optimal" at one given time, and no evidence of their efficiency for other times is raised.

Comparing different methods for the inversion of the LT is an alluring prospect. An interesting comparison was accomplished by Duffy [24], where Talbot's method compteted with Weeks's method and the direct method. The outcome was that in most cases, Talbot's algorithm is superior. However, it is not suitable for transforms with singularities that have an imaginary part growing to infinity, which is quite predictable, but less predictable is its relative failure to approximate functions having singularities lying on the Fourier axis (for instance, the Bessel function above). In [86, 68], the auhtors compared parametrized Bromwich contours to rational approximations; see also [36]. Actually, starting from the observation that any quadrature formula applied to the inversion of the LT could be viewed as a rational approximation, they compare the Talbot method (using various

contours: parabola, hyperbola, cotangent) to the method devised by Cody, Meinardus & Varga [18]. The results are mixed: best rational approximations are twice as fast compared to Talbot contours, however these are simpler to implement. Moreover, if parameters are to be tuned for the inversion at a given time, the accuracy of the first method is harder to maintain on an interval containing that point in time. As a conclusion, the best rational approximations method seems hardly suitable for an inversion on a whole interval of time.

1.1.2 Hyperbolic contour vs. sinc approximations

As of late, there has been a wealth of litterature dealing with the numerical inversion of the LT via quadratures using Talbot contours. This interest seems to have have been kicked off with the master thesis of López-Fernández [47], which was in turn followed by some papers focusing on the optimization of the quadratures involved for the numerical inversion per se. Indeed, in [48], López-Fernández & Palencia use a quadrature formula based on the sinc function. In practice, they use the trapezoidal rule to discretize the integral written on a hyperbolic contour, see Figure 5. The singularities of the integrand are assumed to lie in an acute sector $\sum_\delta = \{s \in \mathbb{C} : |\arg(-s)| \leq \delta\}$, see Figure 3. Moreover, the integrand admits a holomorphic extension $\Delta_d = \{s \in \mathbb{C} : |\Im s| < d\}$ outside the latter sector. Thence, they set out to obtain an accurate estimate to the quadtrature error, that is, the absolute difference between the real LT inverse and the truncated trapezoidal approximation. To do so, they improve an interesting estimate due to Stenger [71, 72]. In effect, Stenger's work deals with the approximation of analytical functions derived via Whittaker's cardinal function. Namely, if f is a function defined on the real line, the cardinal function is defined by

$$C(f,h) = \sum_{k=-\infty}^{\infty} f(kh)S(k,h), \tag{7}$$

whenever the series converges, where $h > 0$ is the stepsize,

$$S(k,h)(x) = \frac{\sin[(\pi/h)(x-kh)]}{(\pi/h)(x-kh)}.$$

Now, the relationship between this function and the numerical inversion of the LT is obvious once we observe that

$$\int_{\mathbb{R}} C(f,h)(t)\,\mathrm{d}t = h\sum_{k=-\infty}^{\infty} f(kh).$$

In other words, this "sinc function" expansion of f is closely linked to the trapezoidal approximation of the integral of f. In short, using the properties of the cardinal function, Stenger proves that if f decays rapidly, i.e.,

$$|f| < c\mathrm{e}^{-\alpha|x|},$$

then

$$\Big|\int_{\mathbb{R}} f(x)\,\mathrm{d}x - h\sum_{k=-N}^{N} f(kh)\Big| \leq a\mathrm{e}^{-\sqrt{-2\pi d\alpha N}},$$

where α, a and c are positive reals. The upper estimate was improved in [48] to $\mathcal{O}(\mathrm{e}^{-\gamma\frac{n}{\ln n}})$. Note that, in this work as well as Stenger's the steppsize is fixed in order to minimize the estimate, and the analyticity strip is chosen to be symmetrical which is not a natural assumption. Ultimately, they use the trapezoidal rule on a hyperbola branch fixing the pamameters of the hyperbola so as to fit the sector containing the singularities. The method works for numerical inversions on a bounded time interval starting at $t_0 > 0$. In a subsequent paper [49], López-Fernández, Palencia & Schädle yet improve the error estimate and bring it down to $\mathcal{O}(\mathrm{e}^{-\gamma n})$. This spectral estimate is yielded by

other choices in their previous procedure. The rest of the paper is dedicated to the study of error propagation: a new parameter is introduced in order to halt these. However, the choices made for the free parameters of the problem in general are not "optimal" in any well-defined sense. As a result, one may think that this approach has not been completely understood/exploited at this point.
To conclude, we send the reader interested in sinc approximations to Stenger [73, 74].

1.1.3 Approximation of the LT inverse on an interval

In [64], Rizzardi modifies Talbot's original method for a numerical inversion of the LT on an interval. The underlying principle is to use the same set of values of $F(s)$ on this whole interval, and to make a most judicious choice for the contour's parameters as well. In this fashion, the algorithm may be parallelized. A major drawback of the analysis carried out to optimize the parameters is its assuption that the transform has a finite number of poles that lie in an interval of the Fourier axis. Then, a quite involved analysis of the absolute error between the inverse and its approximation, also invoking the roundoff error, is carried out yielding some optimized contour parameters for an interval $[t_0, t_1]$. The results are quite satisfactory even if error curves display different profiles for different tests, thereby questioning the very consistency of the procedure. However, the author manages honorable results with a small number of evaluations of $F(s)$, i.e. N, but then again the test functions do not display the nonstandard features, such as cuts and branchpoints, actually encountered in realistic models; see [24].

We think that a major breakthrough in the contour deformation technique was achieved recently by Weideman & Trefethen [85]. Indeed, these authors propose a procedure of optimization of two "simple" smooth Bromwich contours (a parabola and a hyperbola) for an approximation of the inverse function on an interval; see section 2. The incentive behind their paper [85] seems to be the recent resurgence of interest that this topic has instigated lately; see [77] and the recent references in the two subsections above as well as the references therein. In fact, the origin to their result seems to be [86], where the first author addressed the particular problem of solving parabolic PDEs using Talbot quadratures (see paragraph 1.1.1), and [77] where the authors take a glance at the stability of the tuned parameters on an interval of time. Still, some issues linger on such as the complete optimization of the position of the contours, and the related problem of approximating transforms exhibiting singularities on the Fourier axis. A thourough study of his method was the subject of this report. We shall also compare it to the approximation of diffusive representations method.

1.2 Approximating exact diffusive representations

In this paragraph, we shall briefly present another approach to the numerical inversion of the Laplace transform that is quite efficient at a low cost. For the sake of clarity, we choose to present the method on an elementary example; we send the reader to [41] for a full treatment of the general case, see also the refrences therein.

Integral representations on cuts We consider the classical integral operator of fractional order equal to $\frac{1}{2}$ whose irrational transfer function is:

$$H(s) = \frac{1}{\sqrt{s}}.$$

This operator cannot be represented by a series of first-order systems, however it may be exactly respresented by a continuous superposition of first-order systems known as *diffusive representation*.

But first, let us note that the above complex function is singular at 0, and in addition, if we parametrize the Laplace variable s in this fashion

$$s = \rho\, \mathrm{e}^{\imath\, \phi}, \quad \phi \in (\theta - 2\pi, \theta],$$

then

$$\sqrt{s} = \sqrt{\rho}\, \mathrm{e}^{\imath\, \frac{\phi}{2}},$$

so that we necessarily have to choose a cut $\mathcal{C}_\theta$ at the branchpoint $s = 0$ for continuity reasons. Now if we choose the cut $\mathcal{C}_\pi$, for instance, we obtain the following realization of the function as

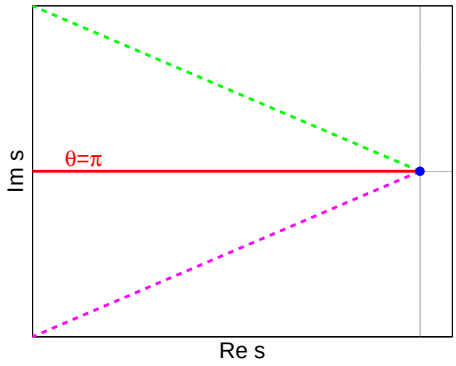

Figure 1: The thick line represents a cut starting at the origin with an angle $\theta = \pi$. Dashed lines represent other possible cuts taken at different angles.

an integral on the cut:

$$H_\pi(s) = \int_{\mathcal{C}_\pi} \frac{\mu_\pi(\xi)}{s + \xi}\, \mathrm{d}\, \xi$$

where

$$\mu_\pi(\xi) = \lim_{\eta \to 0^+} \frac{H_\pi(-\xi + \imath\, \eta) - H_\pi(-\xi - \imath\, \eta)}{2\imath\pi}. \tag{8}$$

Note that a technical well-posedness condition has to be imposed upon the weight μ_π, at least for the integral to make sense. We shall not expose this issue here since this is not our purpose. Furthermore, this approach has been extensively studied and presented in the litterature. We would like to mention that the expression (8) above is sometimes referred to as the Henrici formula; see [20]. Now,

$$H_\pi(s) \quad \xrightarrow{\mathcal{L}^{-1}} \quad h(t),$$

so that h is the unit impulse function computed as the inverse Laplace transform of H_π. Hence, to obtain a time response with respect to an entry signal u one has to convolute with h:

$$y(t) = h * u(t).$$

The corresponding operator admits a simple diagonal realization in systems theory as follows:

$$\partial_t \phi(\xi, t) = -\xi \phi(\xi, t) + u(t), \quad \xi \in \mathbb{R}^+,$$
$$y(t) = \int_0^{+\infty} \phi(\xi, t) \mu_\pi(\xi) \mathrm{d}\xi,$$

where the operator is realized through solving the above infinite set of linear PDEs first, followed by a weighted integration the weight of which depends upon the choice of the cut.

Numerical approximation The above realization is approximated by a finite-dimensional model:

$$\widetilde{H}_\mu(s) = \frac{1}{2}\sum_{n=0}^{N}\left[\frac{\mu_n}{s-\gamma_n} + \frac{\overline{\mu_n}}{s-\overline{\gamma_n}}\right],$$

where only a finite set of poles (singularities) γ_n on the cut are considered. Then, weights μ_n are optimized through the weighted least-squares criterion below:

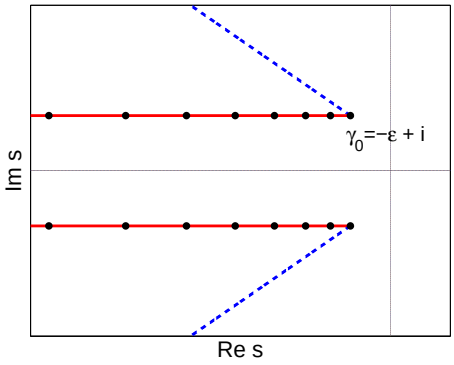

Figure 2: Logarithmic distribution of nodes on the two horizontal cuts starting at branchpoints $-\varepsilon \pm \imath$. Dashed half lines represent alternative cuts.

$$\mathcal{C}(\mu) \triangleq \int_{\mathbb{R}^+} \left|\widetilde{H}_\mu(2\imath\pi f) - \widehat{J^\varepsilon}(2\imath\pi f)\right|^2 w(f)\,\mathrm{d}f,$$

where some choices are made heuristically, but based on psychoacoustics, and audio performance for our purpose. The advantage of such a method is its effeciency with a very limited number of poles, i.e., numerically speaking, a small number of nodes. This method seems to have been first employed in Garcia & Bernussou [32], then put in a more rigorous framework by Dunau & Montseny. Hélie & Matignon have been doing a lot of testing and have well-tuned the heuristic over the years; see [39, 37, 38]. We send the reader to section 4 for a more specific presentation of the procedure.

1.3 Other methods

Over the years, the numerical inversion of the Laplace transform has summoned the attention of many a mathematician. The approaches have been varied either theoretically or numerically. Some research attempted finding analytical ways of circumventing the difficulty of approximating the Bromwich integral. These efforts more often than not concerned very particular problems like fractional kinetic equations [11], luminescence spectroscopy [12], or the Boltzmann equations in a very specific framework [14, 13]. Others obtained results for Green functions with a discrete set of poles (i.e. no cuts or branchpoints) [20, 43].

A more straightforward way of tackling the numerical integration is through a mere approximation of the integral through the Fourier series of the Laplace transform [21], which amounts more or less to the straightforward application of the trapezoidal rule to the Bromwich integral; see also [58].

Another successful approach is known as the Weeks method, and is the paradigm for what is known as the collocation methods. The general idea underlying these schemes is to approximate the inverse as an expansion on some special set of functions; namely, Weeks [84, 34] suggested the Laguerre polynomials because the quadrature formulas are similar to the Laplace transform

operator which kicked off probably the most notorious direction of research in this field by trying other approximation functions with slight variants in the framework ([59]); see also [17, 67].

More exotic attempts have been made. These include the Gaver-Stehfest method [80], the power method [8, 7], the direct method of Schapery [17, 67]. There are also schemes that combine several of these ideas [1] without sensitive improvements.

To conclude this paragraph, we shall say that the general drawback in these methods is that very often costly regularizations ([19]) and accelerations ([3]) are required, and free parameters have to be heuristically tuned rendering the resulting schemes hardly implementable in an automatic and cheap fashion. What is more, improving the efficiency of such algorithms is quite involved.

Remark 1.1. Note that despite the fact that some of these algorithms are almost automatic, they usually compute the value of the inverse at a given time so that these have yet to be optimized for the computation of the time response at *any* time, or in a given *interval* of time.

2 Optimized Bromwich contours

Contours We set to study and implement two parametrized Bromwich contours following Weideman & Trefethen [85]. Indeed, these contours seem to have produced the best results known for a very quick automatic numerical inversion of the LT on an interval.

The first contour is the parabola:

$$\gamma(u) = \mu(\imath\, u + 1)^2 + \beta, \tag{9}$$

and the second one is the hyperbola

$$\gamma(u) = \mu(1 + \sin(\imath\, u - \alpha)) + \beta, \tag{10}$$

where $u \in]-\infty, \infty[$, $\mu > 0$ regulates the width of the contours, β determines their foci, and α defines the hyperbola's asymptotic angle. Note that the motivation for these choices is their simplicity and suitability for a trapezoidal approximation (4); in both cases, γ is a smooth conformal map. In particular, the cotangent contour (5) originally proposed by Talbot is quite difficult to analyze; see [75, 86, 64]. These simpler contours have been introduced most recently. The parabolic contour (9) first appeared in [33], where the optimization of the contour relied on arguments related to the sinc quadratures used in their algorithm following [73]; see also paragraph 1.1.2. As for the hyperbolic contour (10), it was first used in [70] where no explicit mention of an optimization of the contour is made. Then, [48] the contour is somewhat optimized using arguments from sinc approximation theory [71, 72]; see paragraph 1.1.2 for more details on this approach.

2.1 Error estimates

Following Weideman & Trefethen [85], the optimization of these contours is founded on a balance between the truncation error estimate and the asymptotic error estimate for the trapezoidal rule (4) applied to these contours (9-10).

Truncation error The truncation error is the difference between the infinite series that approximates the inverse (3):

$$F_h(t) = F_{h,\infty}(t) = \frac{h}{2\imath\pi} \sum_{n=-\infty}^{\infty} \mathrm{e}^{\gamma(nh)t} \widehat{F}(\gamma(nh))\gamma'(nh) \approx F(t), \tag{11}$$

and the truncated sum (4). Namely,

$$E_N(t) = |F_h(t) - F_{h,N}(t)|.$$

Now, if $\left|\widehat{F}(\gamma(s))\right|$ decays rapidly as $|s| \to \infty$, the truncation error may be assumed to behave like the magnitude of the last term in the sum (4), i.e.,

$$E_N(t) = \mathcal{O}(|\, h\mathrm{e}^{\gamma(Nh)t}\, \widehat{F}(\gamma(Nh))\, \gamma'(Nh)\,|), \tag{12}$$

since the next terms are

Asymptotic error Also called dicretization error, it is the difference between the inverse LT $F(t)$ and the infinite trapezoidal approximation (11), i.e., $E_h(t) = |F(t) - F_h(t)|$. To obtain quite a sharp estimate of this error, some complex analysis is needed. Indeed, here is the fundamental result, almost as stated in Theorem 2.1. in [85], we shall use to accurately assess this error.

Theorem 2.1. Let $f : \mathbb{R} \to \mathbb{R}$ be a function analytic in $\mathcal{U} = \{s \in \mathbb{C} : -c^- < \Im(s) < c^+\}$, where $c^\pm \geq 0$, and $f(s) \to 0$ uniformly as $|s| \to \infty$ in $\mathcal{U}$. Furthermore, assume that $f(s)$ satisfies

$$\int_{-\infty}^{\infty} |f(u+iv)|\mathrm{d}u \leq M^+ \quad \text{and} \quad \int_{-\infty}^{\infty} |f(u-iw)|\mathrm{d}u \leq M^-, \quad \forall\, 0 < v < c^+,\ 0 < w < c^-,$$

where $M^\pm > 0$. Then

$$\left| \int_{-\infty}^{\infty} f(u)\mathrm{d}u - h \sum_{k=-\infty}^{\infty} f(kh) \right| \leq E_h^+ + E_h^-, \quad E_h^\pm = \frac{M^\pm}{\mathrm{e}^{2\pi c^\pm/h} - 1}. \tag{13}$$

Remark 2.1. A few remarks regarding this result have to be made:

1. The function $f(u)$ is real and admits a holomorphic extension to $\mathcal{U}$. In practice, if we consider

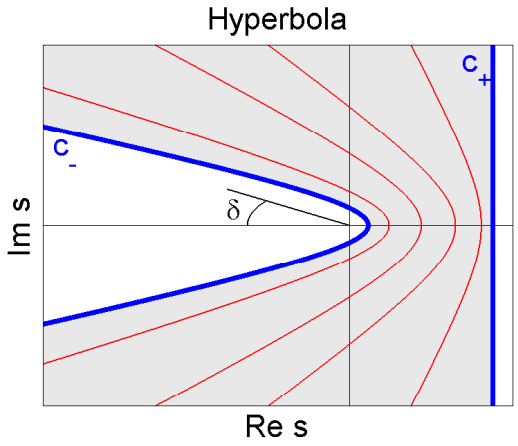

Figure 3: Strip of analyticity

the hyperbola, for instance,

$$\gamma(v) = \mu(1 + \sin(\imath\, v - \alpha)),$$

for the inversion of a function whose singularities lie in a sector defined by the angle δ, see Figure 3, and take

$$v = u + \imath\, c, \quad u \in \mathbb{R},$$

then as c spans the interval $[-c_-, c_+]$, the hyperbolic contour sweeps the grey area that goes from the hyperbola embracing the sector in the left halfplane to the vertical line in the right halfplane.

2. For our purpose, the function f will be of the form

$$f(u) = \frac{1}{\imath 2\pi} e^{\gamma(u)t} \hat{F}(\gamma(u))\gamma'(u)$$

so that the estimated truncation/asymptotic errors will depend on both: the chosen contour $\gamma(\mathbb{C})$, the instant t, and, consequently the time interval $[t_0, t_1]$ if need be.

3. Classically, in the litterature [40, 69], the analyticity strip is taken to be symmetric $c^+ = c^-$, which reduces the estimate (13) to the more familiar inequality known in numerical analysis when f is real-valued.

4. Weideman & Trefethen omitted the proof to this theorem mentioning that "the standard proofs remain essentially the same". However, we do not think that the standard proofs are easy to find or even intuitive. Therefore, we try to give a self-contained proof in the appendix.

2.2 Optimization procedure

The process of the numerical inversion of the LT is done in several steps. First, the appropriate type of contour has to be chosen in accordance with the locus of the singularities of the LT. The parabolic contour (9) is suitable for Laplace transforms with singularities lying on a horizontal half line with real part going to negative infinity as is shown in Figure 4. Whereas the hyperbolic con-

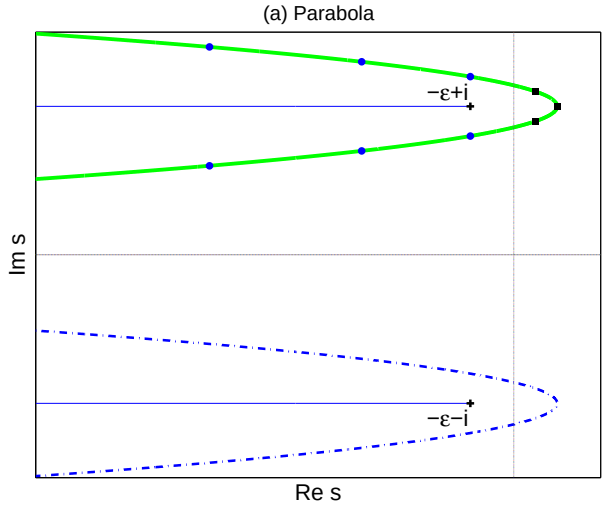

Figure 4: Two parabolic contours optimized for the numerical inversion of the function $\hat{j}_{\pm}^{\varepsilon} = \frac{1}{\sqrt{s+\varepsilon \mp i}}$.

tour (10) is superior in the sense that it is fit for any Laplace transform with singularities lying in a sector in the left halfplane with real part going to negative infinity; see Figure 5. Having chosen the contour, the next move is to obtain the best estimates (12-13) for this particular contour. Namely, the analyticity strip defined in Theorem 2.1 has to be identified. In the cases of interest, the singularities lie in the left halfplane so that c_- is generally finite, whereas c_+ may be infinite. As

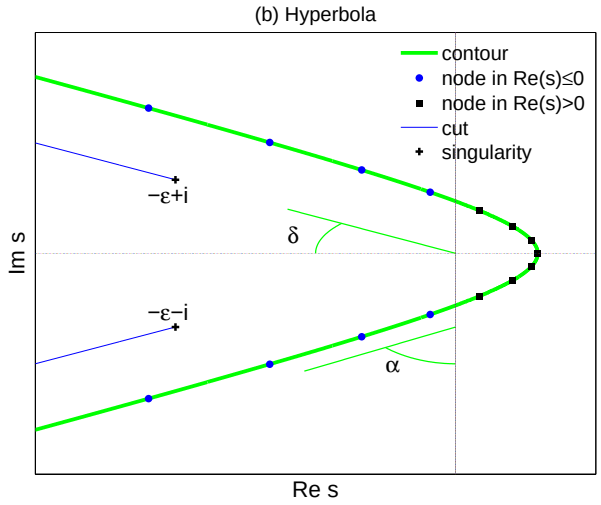

Figure 5: Hyperbolic contour optimized for the numerical inversion of the function $\hat{J}^{\varepsilon} = \dfrac{1}{(s+\varepsilon)^2+1}$. The sector is determined by the angle δ that depends on the position of the singularities $-\varepsilon \mp i$.

it happens, c_+ is infinite for the hyperbolic contour (10) so that the contribution of the exponential term has to be taken into account in order to fix the best strip of analyticity.

Once error estimates for the truncation and discretization have been established, we get an estimate of the absolute error:

$$E(t) = |F(t) - F_{h,N}(t)| \leq E_N(t) + E_h(t).$$

The optimization procedure is quite natural. It consists in choosing to match the estimates at hand (12-13):

$$E_N(t) = E_h^+(t) = E_h^-(t), \tag{14}$$

which yields two equations that should determine an optimal choice of the free parameters μ and h to which we shall refer as μ_* and h_*. One may consider other choices. We shall discuss this issue in the sequel.

Now, equations (14) will optimize the parameters for the time t, and our solutions are to be computed on an interval $[t_0, t_1]$, with $t_1 = \Lambda t_0$. Therefore, Weideman & Trefethen [85] adapt (14) to the interval by taking:

$$E_N(t_0) = E^+ = E_h^-(t_1). \tag{15}$$

The legitimacy of the above condition lies in the expression of these quantities. In fact, the truncation error E_N depends linearly on time, E_h^+ is independent of time, and E_h^- depends linearly on $\dfrac{1}{t}$ for the parabola. Hence the above choice seems sensible to keep these three quantites matched as is the case at one instant t. A similar argument holds for the hyperbolic contour as well.

Indeed, they limit their analysis to the case $\beta = 0$, i.e., the horizontal distance between the contour and the first singularity (6) is not fully *optimized* (cf. this distance is partly regulated by μ too). The authors give no hint as to a preferential choice of $\Re(\beta)$; we shall investigate certain choices in section 3.4. For now, we shall focus on the convergence rates obtained in the above fashion.

Theoretical convergence rates A quite extraordinary occurrence is that the choices made above for an automatic tuning of the contours yield in both cases (parabola and hyperbola) a system of two equations with two unknwons that is analytically resolved in a most simple way. We shall attempt at shedding some light on the *sensitivity* of the process as well as the sensitivity of the contours themselves through simulations.

The optimal contour parameters for the parabola read:

$$h_* = \frac{\sqrt{8\Lambda+1}}{N}, \quad \mu_* = \frac{\pi}{4}\frac{N}{t_1\sqrt{8\Lambda+1}} \tag{16}$$

which entails the convergence rate

$$E_N^\Lambda = \mathcal{O}\big(\mathrm{e}^{(-2\pi/\sqrt{8\Lambda+1})N}\big). \tag{17}$$

As for the hyperbolic contour, the optimal contour parameters read:

$$h(\alpha) = \frac{A(\alpha)}{N}, \quad \mu(\alpha) = \frac{4\pi\alpha - \pi^2 + 2\pi\delta}{A(\alpha)}\frac{N}{t_1}, \tag{18}$$

$$A(\alpha) = \cosh^{-1}\frac{(\pi - 2\alpha - 2\delta)\Lambda + 4\alpha - \pi + 2\delta}{(4\alpha - \pi + 2\delta)\sin\alpha}, \tag{19}$$

where $\delta \in [0, \frac{\pi}{2}]$ is the angle of the sector defined by the singularities and $\alpha \in [0, \frac{\pi}{2}]$ is the asymptotic angle of the hyperbola, see Figure 5. The resolution of system (15) imposes that the asymptotic angle belongs to a range $\alpha \in [\alpha_0, \alpha_1]$:

$$\frac{1}{2}\big(\frac{\pi}{2} - \delta\big) \le \alpha \le \frac{\pi}{2} - \delta. \tag{20}$$

Accordingly the convergence rate depends on the asymptotic angle:

$$E_N^\Lambda(\alpha) = \mathcal{O}\big(\mathrm{e}^{-B(\alpha)N}\big), \quad B(\alpha) = \frac{\pi^2 - 2\pi\alpha - 2\pi\delta}{A(\alpha)}. \tag{21}$$

Ultimately, the decay rate is maximized (function B posesses a unique local $\bar\alpha$, see Figure (**??**)) so that

$$h_* = h(\bar\alpha), \quad \mu_* = \mu(\bar\alpha), \quad B(\bar\alpha) = \max_{\alpha\in[\alpha_0,\alpha_1]} B(\alpha).$$

Remark 2.2.

1. The first observation is that we can neither consider $t_0 = 0$, nor $t_1 = \infty$. These values either explode the paramters h_* and μ_*, or reduce them to zero.

2. Another preliminary remark is that convergence rates are of the form

   $$E_N^\Lambda = \mathcal{O}\big(\mathrm{e}^{-BN}\big), \quad B > 0.$$

   However, for Λ large we have:

   $$B_{\text{para}} = \mathcal{O}\big(\frac{1}{\sqrt{\Lambda}}\big), \quad B_{\text{hyper}} = \mathcal{O}\big(\frac{1}{\ln\Lambda}\big).$$

   Hence, the supposedly exponential decay may be very costly to maintain on large intervals of time or on intervals. In consequence, if the computation is initiated near zero, it will be hard to have a good convergence rate for large values of time.

3. From the estimates above, one may predict that hyperbolic contours yield more efficient numerical inversions.

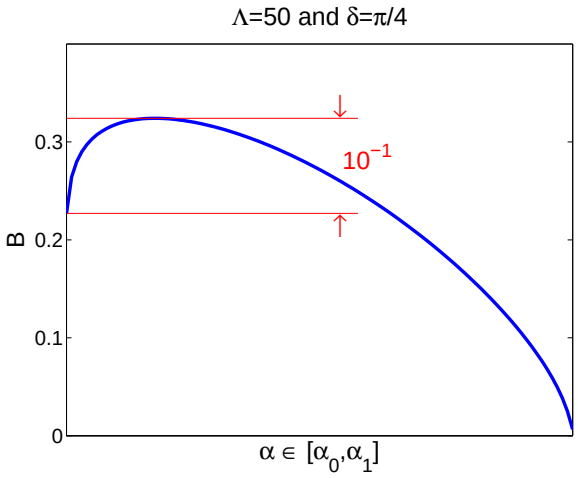

Figure 6: The maximization of function B with respect to asymptotic angle α improves by 10^{-1} the error estimate with respect to $B(\alpha_0)$. We may choose to dispense with this optimization when the rate is already exponential.

3 Numerical results

Numerical simulations have been carried out to compare and outline the limitations of these optimized contours. The test functions are chosen to cover the families of LT that are of interest to our applications. Moreover, the choice is limited to LT the inverse of which is analytically known to be able to compute the numerical error.

Test functions The test functions we have considered for this contour are

$$\widehat{F^1}(s) = \frac{1}{s - s_0}, \quad \Re(s_0) < 0, \qquad F^1(t) = \mathrm{e}^{s_0 t}, \tag{22}$$

$$\widehat{F^2}(s) = \mathrm{e}^{-\sqrt{s}}, \qquad F^2(t) = \frac{\mathrm{e}^{-\frac{1}{4t}}}{2\sqrt{\pi t^3}}, \tag{23}$$

$$\widehat{F^3}(s) = \frac{1}{s^{\frac{1}{2}} - s_0}, \quad \Re(s_0) < 0, \qquad F^3(t) = \frac{1}{\sqrt{\pi t}} + s_0 \mathrm{e}^{s_0^2 t}\,\mathrm{erfc}(-s_0\sqrt{t}), \tag{24}$$

$$\widehat{F^4}(s) = \frac{F_2(s)}{\sqrt{s}} = \frac{\mathrm{e}^{-\sqrt{s}}}{\sqrt{s}}, \qquad F^4(t) = \frac{1}{\sqrt{\pi t}}\mathrm{e}^{-\frac{1}{4t}}, \tag{25}$$

$$\widehat{F^5}(s) = \frac{\tanh(\sqrt{s})}{\sqrt{s}} = \sum_{n\in\mathbb{N}} \frac{2}{s + (n+1/2)^2\pi^2}, \qquad F^5(t) = 2\sum_{n\in\mathbb{N}} \mathrm{e}^{-n^2\pi^2 t}, \tag{26}$$

$$\widehat{F^6}(s) = \frac{1}{\sqrt{s+i}}, \qquad F^6(t) = \frac{\mathrm{e}^{-it}}{\sqrt{\pi t}}. \tag{27}$$

We have tried to span all the types of LT that the parabolic contour may have to deal with. Indeed, this contour is suitable for inverting functions having singularities that lie along a horizontal halfline in the left halfplane. Thence, the choice was motivated by the qualitative differences that may exist. The first function $\hat{F}^1$ has one singularity at $s = -s_0$. The second one $\hat{F}^2$ has a branchpoint that shall be chosen equal to $\mathbb{R}_-$. The third and fourth functions F^3 and F^4 have a pole and a branchpoint each, so cuts have to be chosen. The fifth function F_5 has the same features as the one before; it may be simply represented by a series of first-order systems. The last function F^6 exhibits a branchpoint and a singularity that are not on the negative real axis but on $(i\mathbb{R}^-)$.

3.1 Parabola vs. hyperbola

We have tested the functions above on the same time interval $[t_0, t_1] = [1, 50]$ using the parabolic and hyperbolic contour with $\beta = 0$, as this parameter has not been optimized yet. The results are displayed hereafter where we have plotted the absolute error:

$$\sup_{t\in[t_0,t_1]} |F(t) - F_{h,N}(t)|, \tag{28}$$

as well as the theoretical error estimates obtained above. On each plot of figures 3.1-3.1, we represented these errors for both contours.

The first observation is that for the six tests the estimated errors are guaranteed, therefore the hyperbolic contour yields better convergence rates. Moreover, for both contours, increasing the number of nodes N beyond a certain point is useless. Indeed, for $\Lambda = 50$, we notice that the error does not decrease beyond $N = 50$ for the hyperbolic contour, and $N = 100$ for the parabolic one. In addition, these best rates are comparable which makes the hyperbolic contour twice as fast. These two observations make it quite clear that the hyperbolic contour is to be preferred to the parabolic one.

However, we should mention that the approximation of the first five test functions required only N nodes owing to the hermitian symmetry that reduces the discretization formula to

$$F_{h,N}(t) = \Re\Big[\frac{h}{i\pi}\sum_{n=0}^{N} \mathrm{e}^{\gamma(nh)t}\widehat{F}(\gamma(nh))\gamma'(nh)\Big], \tag{29}$$

as opposed to (4) for the last test function F^6 which actively required $2N$ estimations of the integrand. This is due to the fact that $F^6(t)$ is a complex function whereas the other five inverses are real-valued. In other words, the difference between this function and the others is that the singularities lie on a half line parallel to the negative real axis but distinct from it; see Figure 9. Therefore, the use of the whole contour is hardly avoidable.

For a closer investigation, we plot the evolution of the error in time for a fixed number of nodes $N = 50$. We notice that the approximation starts badly and improves very quickly. More precisely, if we neglect the first 5% of the samples, say $[t_0, t_0'] = [1, 4]$, the error is matched everywhere else, i.e., in $[t_0', t_1]$. This can be viewed in Figure 9.

Remark 3.1. These first computations confirm the superiority of the hyperbolic contour convergence rate wise. Moreover, the flexibility of this contour to fit the singularties thanks to the parameter α which controls the aperture of the branches (10), especially when these have positive and negative imaginary parts as is the case for the Bessel function, make the hyperbolic contour more recommendable for an automatic treatment of the numerical inversion of the LT. Add to this the lower cost of the simulation, and the choice of the hyperbola becomes inevitable. Hence, we shall persue our investigations with the hyperbolic contour.

As further evidence for this choice, we have plot the evolution of the profiles of the errors on the time interval $[1, 50]$ for each contour and each test function. This is displayed in Figures 10 and 11. Note that for each contour, the profiles for each test function seem to globally match. Now, a common feature to both contours is a deterioration of the convergence rate at the end of the interval. However, this phenomenon is progressive over the whole interval and quite relative for the hyperbola. Whereas, the parabolic profile starts with a relatively low convergence rate which improves very quickly, remains stable on half the interval before decreasing as quickly as it has decreased. This is another argument for sticking to the hyperbolic contour.

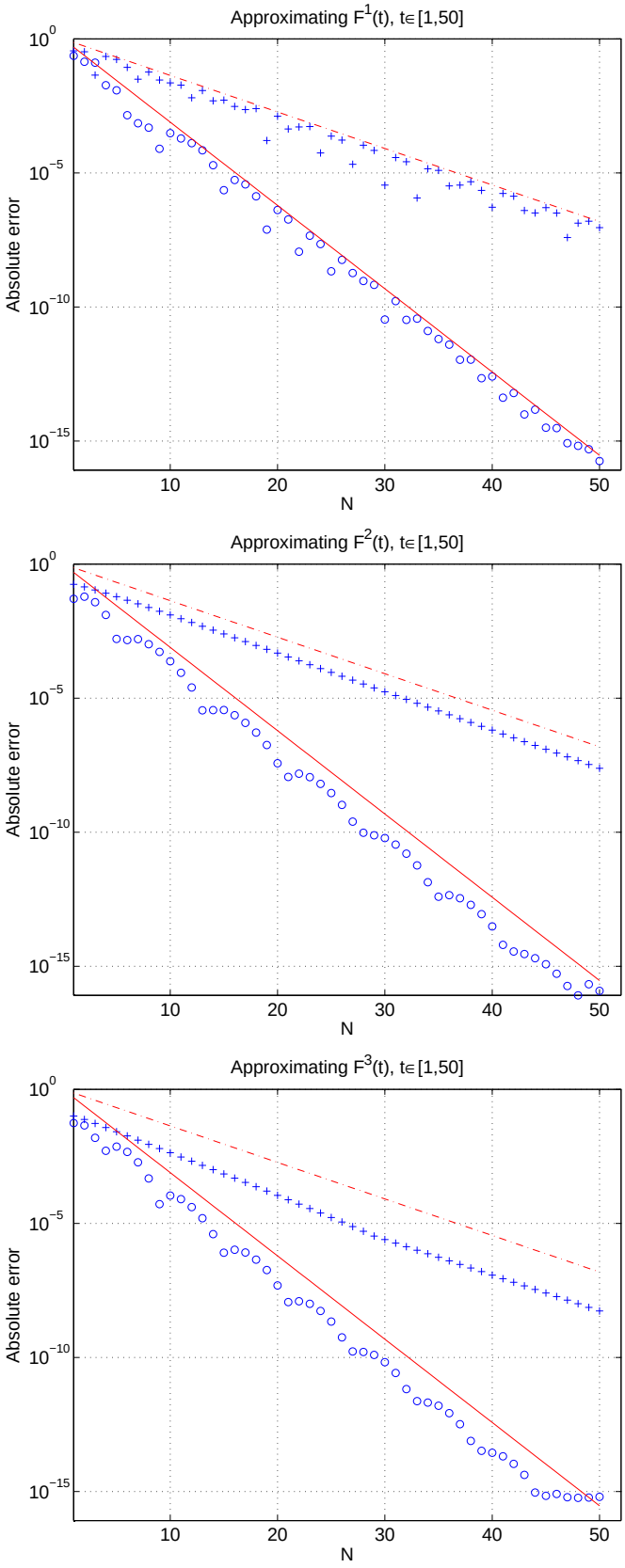

Figure 7: Testing both contours by computing $F^1 - F^6$: The dash-dot line represents the theoretical error using the parabola, while the plus line represents the approximation error ofr the same contour. The full line represents the theoretical error using the hyperbola, and thecircle line the approximation error for this contour.

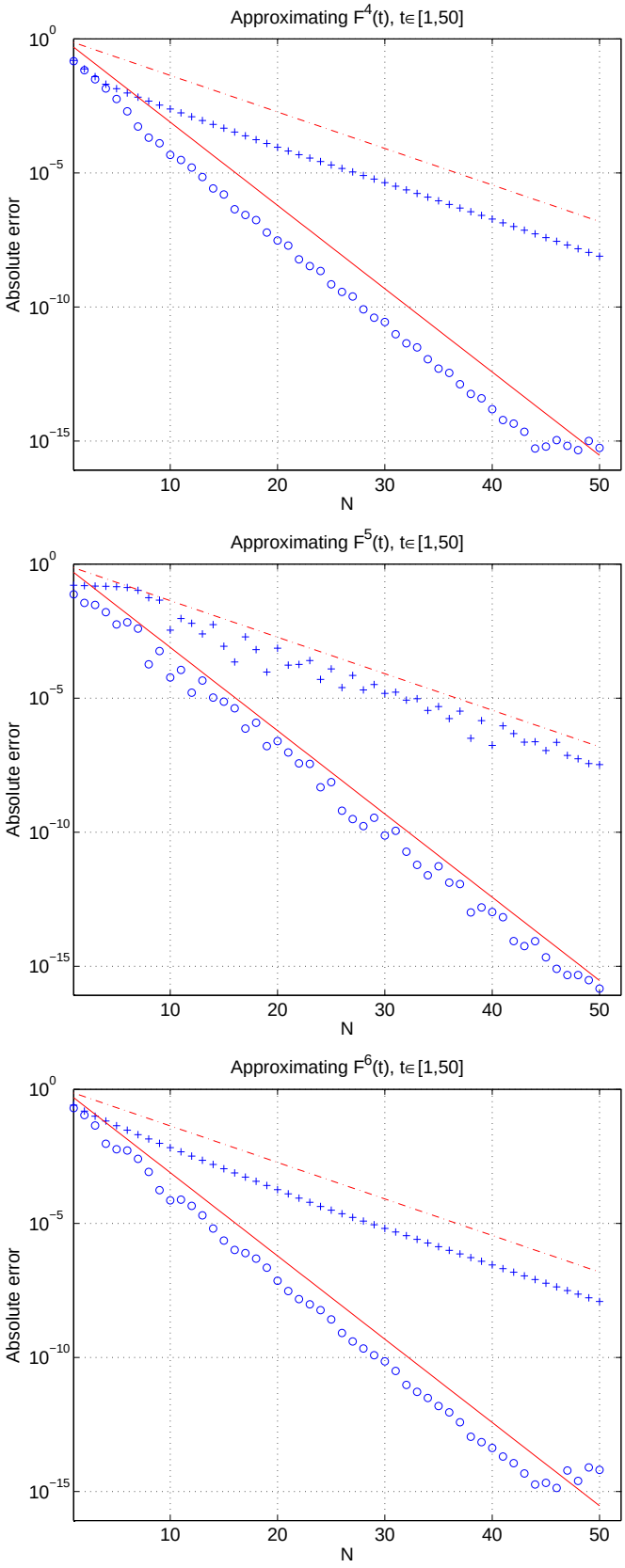

Figure 8: See caption in Figure 3.1.

3.2 Time stability

The issue of time stability is central to the type of problems we are interested in. Actually, long-time decay solutions coming from physical models with realistic damping need time stable methods in

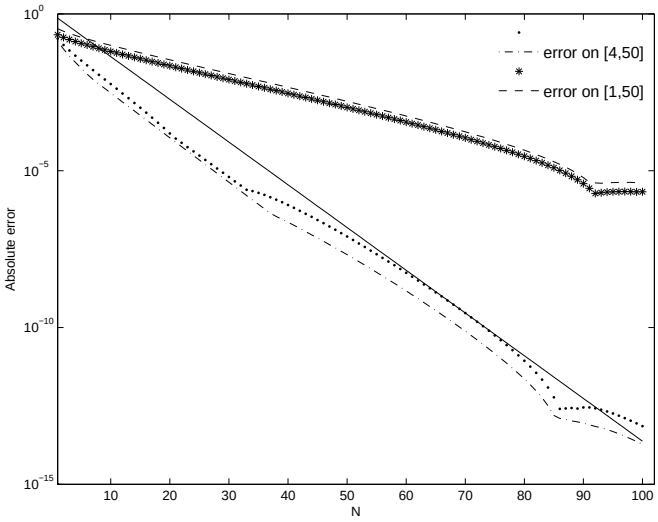

Figure 9: We plot the real and imaginary parts numerical errors in the approximation of f^6. These are computed first on the whole interval of approximation $[t_0, t_1] = [1, 50]$ and are represented by the dashed line and the asterisk respectively, then on a truncated interval ignoring the first 5% samples $[t_0', t_1] = [4, 50]$ by the points and the dash-point line respectively. Note that computations effectively involve the number of nodes N indicated, as the lack of hermitian symmetry does not allow to double the number of nodes, see formula (29).

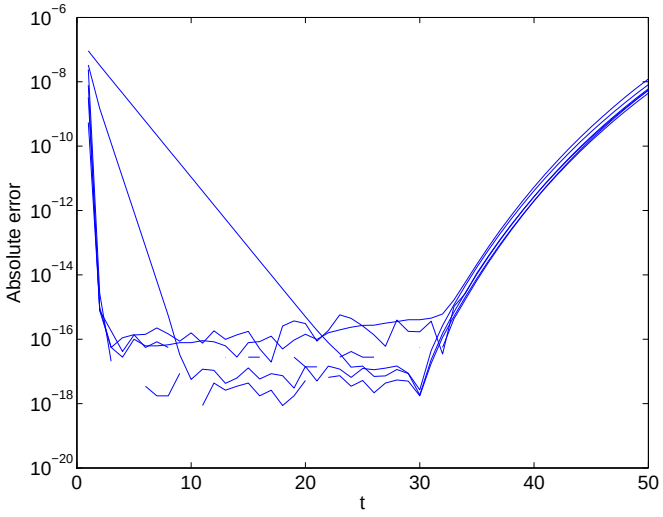

Figure 10: Profile of the error evolution on the time interval $[1, 50]$ in the numerical Laplace inversion of all test functions using a parabolic contour.

order to be simulated over very long time intervals. As for the Talbot contours, the time stability is issue due to the convergence rate which depends in a non trivial fashion on the time interval's diameter Λ; see Remark 2.2. In [85], the question was illustrated for computing the exponential function, i.e., the inverse LT of function $\hat{\hat{F}}_1$; see (22), and the convergence rate decreases as expected.

Here we illustrate this with two test functions displaying cuts. The first function is either one

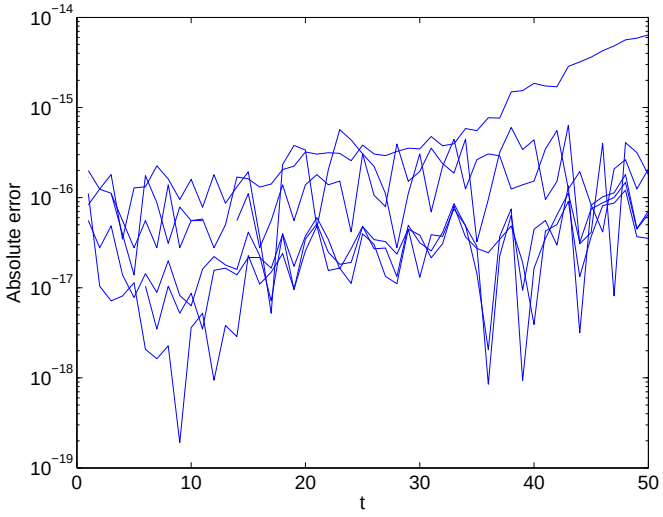

Figure 11: Profile of the error evolution on the time interval $[1, 50]$ in the numercial Laplace inversion of all test functions using a hyperbolic contour.

of the two following functions that are conjugate (and consequently yield identical results):

$$\widehat{j^{\varepsilon}}_{\pm}(s) = \frac{1}{\sqrt{s+\varepsilon \mp \imath}}, \qquad j^{\varepsilon}_{\pm}(t) = \frac{\mathrm{e}^{-\varepsilon t}}{\sqrt{\pi t}} \mathrm{e}^{\pm \imath t}, \tag{30}$$

which have one cut chosen to be $(\pm\imath - \varepsilon\mathbb{R}^{+})$. The second function is a LT of a delayed Bessel function (see Figure 3.2):

$$\widehat{J^{\varepsilon}}(s) = \frac{1}{\sqrt{(s+\varepsilon)^2+1}}, \qquad J^{\varepsilon}(t) = \mathrm{e}^{-\varepsilon\, t}\, J_0(t), \tag{31}$$

which has two branchpoints $-\varepsilon \pm \imath$ at which we choose the cuts to be $(\pm\imath - \varepsilon\mathbb{R}^{+})$. Several tests are carried out to differentiate between the effects: time interval diameter Λ versus cuts.

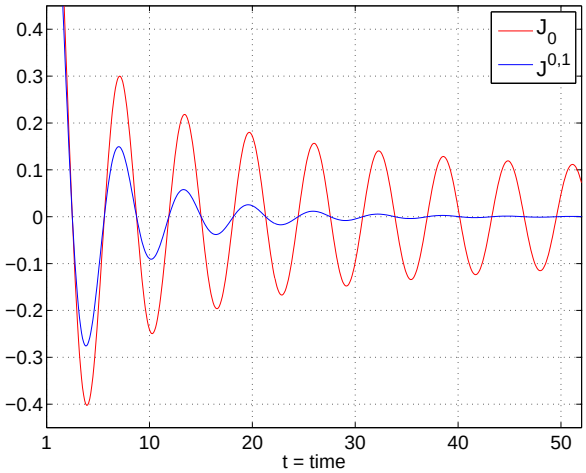

Figure 12: Note that $\varepsilon > 0$ increases the damping.

We first focus on the time stability so that we choose $\varepsilon = 5$: a quite random choice that sends the cuts well into the left Laplace halfplane thereby causing the contours as well to have a negative

real part which makes for a better/more confortable approximation of the integral. We start by a fixed time interval $\Lambda = 10$ as well as a fixed number of nodes $N = 50$ for different starting instants $t_0 \in \{.1, 1, 10\}$. This is produced in Figure 13. The first observation is that the numerical error matches the theoretical one in the inversion of $\widehat{j^\varepsilon}$, which is not the case for $\widehat{J^\varepsilon}$ when $t_0 \in \{.1, 1\}$. The reason for this difference is without a shadow of a doubt to be imputed to the position of the branchpoints on either side of the negative real axis. In what way? is another question. All we can conclude is that for small times, the tuning of the aperture of the hyperbolic contour is very sensitive.

Remark 3.2. Note that the convergence rate, even for the computation of the exponential (see [85]), cannot be improved infinitely by increasing the number of nodes. The problem is ill-conditioned so that the actual error saturates at 30 nodes for $\widehat{j^\varepsilon}$ on a time span equal to 10. Hence, in practice, long time spans should be split into adjacent intervals of equal diameter in order to maintain the desired convergence rate:

$$[t_0, t1] = [t_0, \Lambda t_0] \cup [\Lambda t_0, \Lambda^2 t_0] \cup \cdots \cup [\Lambda^n t_0, t_1].$$

This is not so costly as the parameters are optimized once for all for a fixed time interval diameter Λ. However, this may not be the ideal solution for real-time sound synthesis.

3.3 Position of the contour with respect to the Fourier axis

As we have observed in the previous simulations, the presence of singularities on both sides of the negative real axis seems to seriously perturb the procedure. This is emphasized in Figure 14 where we test the same inversions with $t_0 = 10$ (this eliminates the sensitivity to the small time initialization), and $\varepsilon \in \{0, 1, 3\}$. Again, a singularity on the negative real axis, even if it is on the Fourier axis, does not perturb the procedure as for all positions $\widehat{j^\varepsilon}$ is inverted matching the error estimate. However, such is not the case for the inversion of $\widehat{J^\varepsilon}$ which is very sensitive to proximity of the singularities to the Fourier axis. Actually, for $\varepsilon = 0$, even the error estimate is not good. This is due to the fact that the hyperbola is too wide open so that a lot of nodes have a positive real part on one hand; see Figure **??**. On the other hand, these nodes have large imaginary parts which increase the oscillations of the integrand. This is exactly the opposite of Talbot's intention. To conclude, from $\varepsilon = 0$ to $\varepsilon = 5$ (see Figure 13 and 14), the error estimate improves and the actual error gradually matches the estimated one once the sector the singularities lie in becomes quite acute.

Remark 3.3. One might be tempted to introduce a parameter $\lambda > 0$ in the optimization (15) to try a different match between the asymptotic error and the truncation error. More specifically, for the hyperbola we may choose

$$\lambda E_N(t_0) = E^+ = E_h^-(t_1). \tag{32}$$

Hence, we obtain the following optimized parameters

$$h(\alpha) = \frac{A(\alpha, \lambda)}{N}, \quad \mu(\alpha) = \frac{4\pi\alpha - \pi^2 + 2\pi\delta}{A(\alpha, \lambda)} \frac{N}{t_1}, \tag{33}$$

$$A(\alpha, \lambda) = \cosh^{-1} \frac{(\pi - 2\alpha - 2\delta)\lambda\Lambda + 4\alpha - \pi + 2\delta}{(4\alpha - \pi + 2\delta)\sin\alpha}, \tag{34}$$

yielding the following theoretical error estimate

$$E_N^\Lambda(\alpha, \lambda) = \mathcal{O}\big(\mathrm{e}^{-B(\alpha,\lambda)N}\big), \quad B(\alpha, \lambda) = \frac{\pi^2 - 2\pi\alpha - 2\pi\delta}{A(\alpha, \lambda)}. \tag{35}$$

Now, inspecting the expressions above, function $A(.,\lambda)$ is increasing in terms of λ so that for $\lambda < 1$ the value of A decreases. However, and consequently B increases. However as B is maximized with respect to the asymptotic angle, the maximum of B is not necessarily increased to improve the theoretical error estimate E_N^Λ above. Numerical computations have not risen probing evidence as to the efficiency of such a parameter. If λ is very small or very large, the results deteriorate, whereas for values close to 1, we have not observed any significant pattern. We have also tried another match:

$$E_N(t_0) = \lambda' E^+ = \lambda' E_h^-(t_1), \tag{36}$$

with the same results. We shall address this issue in the future.

3.4 Delaying the functions for a better approximation

At this point, it seems that the proximity of the singularities to the Fourier axis is an important issue. Therefore, we shall eliminate this problem by a mere translation of the singularities farther into the left halfplane in order to minimize their effect on the position and shape of the contour. Practically, a translation of the singularities in the frequency domain by $-\varepsilon$, that we call τ_ε, into the left halfplane induces a delay in the time response in the form of an exponential damping by exactly $\mathrm{e}^{-\varepsilon t}$. Hence, one might be tempted to make the inversion after the translation, and restore the initial time domain response by multiplying the approximation by $\mathrm{e}^{\varepsilon t}$. The idea being that if at the instant $t > 0$,

$$|(\tau_\varepsilon F)_{h,N}(t) - \tau_\varepsilon F(t)| = \mathcal{O}(\mathrm{e}^{-BN}),$$

then

$$\left|\mathrm{e}^{\varepsilon t}(\tau_\varepsilon F)_{h,N}(t) - F(t)\right| = \mathcal{O}(\mathrm{e}^{(-B+\varepsilon)N}),$$

since

$$F(t) = \mathrm{e}^{\varepsilon t}\mathcal{L}^{-1}[\tau_\varepsilon \hat{F}(s)](t).$$

And we expect the rate $-B + \varepsilon$ to be better than the one we would have by inverting directly $\hat{F}$ instead of $\tau_\varepsilon \hat{F}$. Globally, this procedure should improve the ill-conditioning of the numerical integration. As a test, we shall deduce the first kind Bessel function of order 0, J_0, from the numerical approximation of $\widehat{J^\varepsilon}$. We recall that, in the previous section, the Bessel function was difficult to approximate accurately, whereas the delayed function was approximated with very low numerical errors; see Figure 14.

As an illustration of this "trick", we have computed the Bessel function J_0 and the functions $j_\pm^0$ on the time interval $[.1, 100]$, i.e., $\Lambda = 100$ by deducing them from the approximations obtained for $\widehat{J^\varepsilon}$ and $\widehat{j^\varepsilon}$, $\varepsilon \in \{10^2, 10^3, 10^4\}$: see Figure 15. The improvement of the numerical error is not significant if the singularities are *sent farther*.

The result is very satisfying: we have clearly solved the problem of the proximity of the singularity to the Fourier axis. Now, all error estimates are matched by tha approximations. What is more, we have even managed to treat large time intervals. Actually, the interesting feature is that we do not really improve the error estimate for $j_\pm^0$, whereas not only the error is matched for the Bessel function but it is even slightly improved for large values of ε!

The effect of the parameter β Note that Weideman & Trefethen [85] are very expeditious about the subject. While it is clear that the error is expected to be multiplied by $\mathcal{O}(\mathrm{e}^{\Re\beta t})$ at any given time t, the effect of such a translation of the contour is not explicit. In practice, if $\Re\beta > 0$, the approximation rapidly degenerates as a larger number of nodes has positive real parts, even if the effect is not so direct: $\Re\beta > 0$ means that the hyperbolic contour is moved away from the eventual singularities which has the effect of reducing the angle of the sector where these are enclosed. In turn, this will not decrease the number of nodes in the right halfplane, however the imaginary part

of these nodes will be reduced tempering the oscillations of the integrand. This effect is numerically observed in the approximation of the exponential:

Absolute error	β	Nodes in $\Re(s) > 0$
10^{-16}	0.5	17
10^{-10}	0.25	13

where, despite a larger number of nodes with positive real part for $\beta = \frac{1}{2}$, the absolute error is sensitively better than in the contrary the other case.

Now, as already emphasized in this section, a problematic approximation is due to the proximity of the singularities to the Fourier axis. In this case, moving the hyperbola to the right of the imaginary axis won't solve the problem. Hence, we have decided to optimize the approximation procedure described above by taking $\Re\beta < 0$ in the approximation of the delayed function as the singularities have large negative real parts. Practically, we have computed J_0 and $j_\pm^0$ again on the time interval $[.1, 100]$ by, first, moving far away the singularities by taking $\varepsilon = 10^5$ and testing $\Re\beta \in \{0, -10^2, -10^3\}$. The results are explicit: it is very interesting to move the contour to the left whenever possible, i.e., whenever this action does not bring it too close to the singularities.

4 Parametrized contours vs. optimal integral representations

The transfer function $\widehat{J^\varepsilon}(s)$ is analytic in the Laplace domain $\Re\mathrm{e}(s) > -\varepsilon$. In this section, we consider analytic continuations $\widehat{J_\theta^\varepsilon}$ of $\widehat{J^\varepsilon}$ over $\mathbb{C} \setminus (\mathcal{C}_\theta \cup \overline{\mathcal{C}_\theta})$, with the cuts $\mathcal{C}_\theta = \left(\imath - \varepsilon + \mathrm{e}^{\imath\theta}\mathbb{R}^+\right)$ and $\overline{\mathcal{C}_\theta}$, and $\widehat{J_\theta^\varepsilon}$ defined by:

$$\begin{aligned} \widehat{J_\theta^\varepsilon}(s) &= \frac{1}{\sqrt[(\theta)]{s+\varepsilon-\imath}\ \sqrt[(2\pi-\theta)]{s+\varepsilon+\imath}}, \\ \sqrt[(\theta)]{\rho\,\mathrm{e}^{\imath\phi}} &= \sqrt{\rho}\,\mathrm{e}^{\imath\phi/2},\ \text{if } \rho \geq 0,\ \phi \in]\theta - 2\pi, \theta[. \end{aligned} \tag{37}$$

4.1 Principle

For $u \geq 0$, let $\gamma_u = \imath - \varepsilon + \mathrm{e}^{\imath\theta}u$ be a parametrization of $\mathcal{C}_\theta$. Function $\widehat{J_\theta^\varepsilon}(s)$ has hermitian symmetric decomposition $\left(\widehat{J_\theta^{\varepsilon^+}}(s) + \overline{\widehat{J_\theta^{\varepsilon^+}}(\overline{s})}\right)/2$, with integral representation:

$$\begin{aligned} \widehat{J_\theta^{\varepsilon^+}}(s) &= \int_{\mathcal{C}_\theta} \frac{\mu_\theta(\gamma)}{s-\gamma}\,\mathrm{d}\gamma = \int_{\mathbb{R}^+} \frac{\mu_\theta(\gamma(u))}{s-\gamma(u)}\gamma'(u)\,\mathrm{d}u, \\ \mu_\theta(\gamma_u) &= \lim_{\eta\to 0^+} \frac{H_\theta\left(\gamma_u + \imath\gamma_u'\eta\right) - H_\theta\left(\gamma_u - \imath\gamma_u'\eta\right)}{2\imath\pi} \\ &= \left[\pi\sqrt{u}\ \sqrt[(\theta)]{2\imath + \mathrm{e}^{\imath\theta}u}\right]^{-1} \mathrm{e}^{\imath\frac{\pi-\theta}{2}} \end{aligned} \tag{38}$$

which fulfills the well-posedness criterion (see e.g. [**?**]):

$$\int_{\mathcal{C}_\theta} \left|\frac{\mu(\gamma)\,\mathrm{d}\gamma}{1-\gamma}\right| \triangleq \int_{\mathbb{R}^+} \left|\frac{\mu(\gamma_u)}{1-\gamma_u}\gamma_u'\right| \mathrm{d}u < \infty.$$

These systems are approximated by the finite-dimensional models:

$$\widetilde{H}_\mu(s) = \frac{1}{2}\sum_{k=0}^{K}\left[\frac{\mu_k}{s-\gamma_k} + \frac{\overline{\mu_k}}{s-\overline{\gamma_k}}\right], \tag{39}$$

where γ_k are a finite set of poles located on the cut $\mathcal{C}_\theta$. For a given location (so far, only a *heuristic* approach based on Bode diagrams is being used), the weights μ_k are optimized for the weighted least-squares criterion:

$$\mathcal{C}(\mu) \triangleq \int_{\mathbb{R}^+} \left| \widetilde{H}_\mu(2i\pi f) - \widehat{J^\varepsilon}(2i\pi f) \right|^2 w(f)\,\mathrm{d}f, \tag{40}$$

with the weight $w(f) = 1_{[f^-,f^+]}(f)/(f\,|\widehat{J^\varepsilon}(2i\pi f)|^2)$. The latter takes into account a bounded frequency range, a logarithmic frequency scale, and a relative error measurement (see [**?**] for details). Note that the Laplace transform of (4) is of the form (39) with $\gamma_k = \gamma(kh)$ and $\mu_k = 2h\gamma'(kh)\,\widehat{J^\varepsilon}\big(\gamma(kh)\big)$ for $0 \le k \le K = N$.

4.2 Numerical results

We consider four cases: **(C1)** J^0 with $\theta = \pi$, **(C2)** J^1 with $\theta = \pi$, **(C3)** J^0 with $\theta = \frac{\pi}{2}$, **(C4)** J^1 with $\theta = \alpha + \frac{\pi}{2}$; see Figure 17. Results are presented on Fig. **??** for poles ($1 \le K \le 8$) on $\mathcal{C}_\theta$ with log-spaced u from $u_{min} = 5.10^{-4}$ to $u_{max} = 5.10^3$. Note that horizontal cuts (i.e. $\theta = \pi$) improve the approximations significantly. In a certain sense, we may think that this improves the approximation of the integral in the same fashion devised by Talbot. Another important remark is that these approximations are time stable.

Comapring with the results obtained for hyperbolic contours, one might first of all remark that singularities on the Fourier axis are an issue for this method too. With more nodes, the parametrized contours manage a slightly better result. Whereas, for the approximation of J^1, this method seems more successful, requiring less nodes $N = 8$, instead of $N = 40$ for the hyperbolic contour, to produce an error of 10^{-4}; see Figure 19. However, once we use the trick of moving the singularities away to the left, the hyperbolic contour becomes significantly more efficient even with a very small number of nodes.

5 Conclusion

From the testing of the parametrized contours carried out here, we first incur that their optimization has not been as yet completely understood. As already observed, there seems to be a minimal distance to the singularities that the contour cannot go beyond without degenerating the scheme. A solution would be to move away the singularities into the left halfplane as we did, which, the least we can say, works pretty well. Still, even if we minimize the cost of the method nodes wise, the lack of time stability is a serious drawback for real-time sound synthesis. As for the optimal integral representations, despite being time stable, they do not provide convergence rates as fast as those obtained by a hyperbolic contour. This is a serious limitation due to the very nature of the method. In addition, no error estimates are available so far.

Acknowlegement I would like to thank the CONSONNES project (ANR-05-BLAN-0097-01) for supporting my research during the 2006-2007 academic year. I should also thank Thomas Hélie and Denis Matignon for introducing me to a mathematical field that was unknown to me up till then.

6 Bibliography

[1] Joseph Abate and Ward Whitt. A unified framework for numerically inverting Laplace transforms. *INFORMS J. Comput.*, 18(4):408–421, 2006.

[2] K. Adolfsson, M. Enelund, and S. Larsson. Adaptive discretization of fractional order viscoelasticity using sparse time history. *Comput. Methods Appl. Mech. Engrg.*, 193(42-44):4567–4590, 2004.

[3] Jaemin Ahn, Sungkwon Kang, and YongHoon Kwon. A flexible inverse Laplace transform algorithm and its application. *Computing*, 71(2):115–131, 2003.

[4] Grégoire Allaire. *Analyse numérique et optimisation*, volume 58 of *Éditions de l'École Polytechnique*. Editions Ellipses, Paris, 2005.

[5] Grégoire Allaire and Alan Craig. *Numerical Analysis and Optimization*, volume 58 of *Numerical Mathematics and Scientific Computation*. Oxford University Press, New York, 2007. Oxford Science Publications.

[6] J. Audounet, D. Matignon, and G. Montseny. Opérateurs différentiels fractionnaires, opérateurs pseudo-différentiels, représentations diffusives. In GdR ISIS, editor, *Journées opérateurs pseudo-différentiels et représentations diffusives en modélisation, contrôle et signal, LAAS/CNRS*, Journées Thématiques, page 10, Toulouse, France, November 1999. SMAI, INRIA.

[7] E. Avdis and W. Whitt. Supplement to "power algorithms for inverting Laplace transforms", 2006. Supporting material for "Power algorithms for inverting Laplace transforms".

[8] E. Avdis and W. Whitt. Power algorithms for inverting Laplace transforms. *Inf. J. Comput.*, 19(3):341–355, 2007.

[9] L. Baratchart, A. Ben Abda, F. Ben Hassen, and J. Leblond. Recovery of pointwise sources or small inclusions in 2D domains and rational approximation. *Inverse Problems*, 21(1):51–74, 2005.

[10] Mário N. Berberan-Santos. Analytical inversion of the Laplace transform without contour integration: application to luminescence decay laws and other relaxation functions. *J. Math. Chem.*, 38(2):165–173, 2005.

[11] Mário N. Berberan-Santos. Properties of the Mittag-Leffler relaxation function. *J. Math. Chem.*, 38(4):629–635, 2005.

[12] Mário N. Berberan-Santos. Relation between the inverse Laplace transforms of $I(t^\beta)$ and $I(t)$: application to the Mittag-Leffler and asymptotic inverse power law relaxation functions. *J. Math. Chem.*, 38(2):265–270, 2005.

[13] A. V. Bobylev and C. Cercignani. Exact eternal solutions of the Boltzmann equation. *J. Statist. Phys.*, 106(5-6):1019–1038, 2002.

[14] A. V. Bobylev and C. Cercignani. The inverse Laplace transform of some analytic functions with an application to the eternal solutions of the Boltzmann equation. *Appl. Math. Lett.*, 15(7):807–813, 2002.

[15] S. Chaabane, I. Fellah, M. Jaoua, and J. Leblond. Logarithmic stability estimates for a Robin coefficient in two-dimensional Laplace inverse problems. *Inverse Problems*, 20(1):47–59, 2004.

[16] Y. Chen, I. Petras, and B. Vinagre. A list of Laplace and inverse Laplace transforms related to fractional order calculus. Available at http://www.steveselectronics.com/petras/foc_laplace.pdf, 2001.

[17] R. M. Christensen. *Theory of viscoelasticity (2nd edition)*. Academic Press, New York, 1982.

[18] W. J. Cody, G. Meinardus, and R. S. Varga. Chebyshev rational approximations to e^{-x} in $[0, +\infty)$ and applications to heat-conduction problems. *J. Approximation Theory*, 2:50–65, 1969.

[19] S. Cuomo, L. D'Amore, A. Murli, and M. Rizzardi. Computation of the inverse Laplace transform based on a collocation method which uses only real values. *J. Comput. Appl. Math.*, 198(1):98–115, 2007.

[20] L. D'Amore, A. Murli, and M. Rizzardi. An extension of the Henrici formula for Laplace transform inversion. *Inverse Problems*, 16(5):1441–1456, 2000.

[21] Luisa D'Amore, Guiliano Laccetti, and Almerico Murli. An implementation of a fourier series method for the numerical inversion of the Laplace transform. *ACM Trans. Math. Softw.*, 25(3):279–305, 1999.

[22] François Dubois and Stéphanie Mengué. Schémas numériques implicites pour les équations semi-différentielles. Technical report, IAT – CNAM internal report, 2000.

[23] François Dubois and Stéphanie Mengué. Mixed collocation for fractional differential equations. *Numer. Algorithms*, 34(2-4):303–311, 2003. International Conference on Numerical Algorithms, Vol. II (Marrakesh, 2001).

[24] Dean G. Duffy. On the numerical inversion of Laplace transforms: comparison of three new methods on characteristic problems from applications. *ACM Trans. Math. Softw.*, 19(3):333–359, 1993.

[25] Dean G. Duffy. *Transform methods for solving partial differential equations*. Chapman & Hall/CRC, Boca Raton, FL, second edition, 2004.

[26] M. Dunau. Représentation diffusive de seconde espèce: introduction et expérimentation. Master's thesis, LASS/CNRS - DEA Systèmes Automatiques, Toulouse, France, 2000. Supervisor: Gérard Montseny.

[27] Mario Durán, Ignacio Muga, and Jean-Claude Nédélec. The Helmholtz equation with impedance in a half-plane. *C. R. Math. Acad. Sci. Paris*, 340(7):483–488, 2005.

[28] Mario Durán, Ignacio Muga, and Jean-Claude Nédélec. The Helmholtz equation with impedance in a half-space. *C. R. Math. Acad. Sci. Paris*, 341(9):561–566, 2005.

[29] Mario Durán, Ignacio Muga, and Jean-Claude Nédélec. Computing green's function of elasticity in a half-plane with impedance boundary condition. *C. R. Mecanique*, 334:725–731, 2006.

[30] Mario Durán, Ignacio Muga, and Jean-Claude Nédélec. The Helmholtz equation in a locally perturbed half-plane with passive boundary. *IMA J. Appl. Math.*, 71(6):853–876, 2006.

[31] A. C. Galucio, J.-F. Deü, S. Mengué, and F. Dubois. An adaptation of the Gear scheme for fractional derivatives. *Comput. Methods Appl. Mech. Engrg.*, 195(44-47):6073–6085, 2006.

[32] Germain Garcia and Jacques Bernussou. Identification of the dynamics of a lead acid battery by a diffusive model. In *Systèmes différentiels fractionnaires (Paris, 1998)*, volume 5 of *ESAIM Proc.*, pages 87–98. Soc. Math. Appl. Indust., Paris, 1998.

[33] Ivan P. Gavrilyuk and Vladimir L. Makarov. Exponentially convergent parallel discretization methods for the first order evolution equations. *Comput. Methods Appl. Math.*, 1(4):333–355, 2001.

[34] G. Giunta, G. Laccetti, and M. R. Rizzardi. More on the Weeks method for the numerical inversion of the Laplace transform. *Numer. Math.*, 54(2):193–200, 1988.

[35] Houssem Haddar, Thomas Hélie, and Denis Matignon. A Webster-Lokshin model for waves with viscothermal losses and impedance boundary conditions: strong solutions. In *Mathematical and numerical aspects of wave propagation—WAVES 2003*, pages 66–71. Springer, Berlin, 2003.

[36] N. Hale, N. Higham, and L. N. Trefethen. Computing a^α, $\log(a)$ and related matrix functions by contour integrals. *SIAM J. Numer. Anal.,*, 2007. submitted.

[37] Th. Hélie and D. Matignon. Diffusive representations for the analysis and simulation of flared acoustic pipes with visco-thermal losses. *Math. Models Methods Appl. Sci.*, 16(4):503–536, 2006.

[38] Th. Hélie and D. Matignon. Representations with poles and cuts for the time-domain simulation of fractional systems and irrational transfer functions. *Signal Process.*, 86(10):2516–2528, 2006.

[39] Thomas Hélie and Denis Matignon. Numerical simulation of acoustic waveguides for Webster-Lokshin model using diffusive representations. In *Mathematical and numerical aspects of wave propagation—WAVES 2003*, pages 72–77. Springer, Berlin, 2003.

[40] Peter Henrici. *Applied and computational complex analysis. Vol. 2*. Wiley Interscience [John Wiley & Sons], New York, 1977. Special functions—integral transforms—asymptotics—continued fractions.

[41] Héleschewitz. *Analyse et simulation de systèmes différentiels fractionnaires et pseudo-différentiels linéaires sous représentations diffusive*. PhD thesis, Ecole Nationale Supérieure des Télécommunications, Paris, France, December 2000. Supervisor: Denis Matignon.

[42] Deü J.-F. and D. Matignon. A coupled Newmark-diffusive scheme for fractionally damped oscillators. In *Proceedings of the eighth international conference on mathematical and numerical aspects of wave propagation phenomena*.

[43] Jinwoo Lee and Dongwoo Sheen. An accurate numerical inversion of Laplace transforms based on the location of their poles. *Comput. Math. Appl.*, 48(10-11):1415–1423, 2004.

[44] David Levadoux and Gérard Montseny. Diffusive realization of the impedance operator on circular boundary for 2D wave equation. In *Mathematical and numerical aspects of wave propagation—WAVES 2003*, pages 136–141. Springer, Berlin, 2003.

[45] A. A. Lokšin. Wave equations with a singular time delay. *Dokl. Akad. Nauk SSSR*, 240(1):43–46, 1978.

[46] A. A. Lokšin and V. E. Rok. Fundamental solutions of the wave equation with time delay. *Dokl. Akad. Nauk SSSR*, 239(6):1305–1308, 1978.

[47] M. López-Fernández. Inversión numérica de la transformada de Laplace y aplicaciones a problemas de evolución. Master's thesis, Universidad de Valladolid, Valladolid, Spain.

[48] M. López-Fernández and C. Palencia. On the numerical inversion of the Laplace transform of certain holomorphic mappings. *Appl. Numer. Math.*, 51(2-3):289–303, 2004.

[49] María López-Fernández, César Palencia, and Achim Schädle. A spectral order method for inverting sectorial Laplace transforms. *SIAM J. Numer. Anal.*, 44(3):1332–1350 (electronic), 2006.

[50] Francesco Mainardi, Gianni Pagnini, and R. K. Saxena. Fox H functions in fractional diffusion. *J. Comput. Appl. Math.*, 178(1-2):321–331, 2005.

[51] D. Matignon. Stability results for fractional differential equations with applications to control processing. In *Computational Engineering in Systems Applications*, volume 2 of *IMACS*, pages 963–968, Lille, France, July 1996. IEEE–SMC.

[52] D. Matignon. Stability properties for generalized fractional differential systems. In *Systèmes différentiels fractionnaires*, volume 5 of *ESAIM Proc.*, pages 145–158, Paris, France, 1998. Soc. Math. Appl. Indust.

[53] D. Matignon. *Fractals et Lois d'Échelle*, chapter 4, Introduction au calcul fractionnaire, pages 143–184. Traité de Information - Commande - Communication, P. ABRY, P. GONCALVÈS ET J. LÉVY-VÉHEL eds. Hermès edition, 2002.

[54] D. Matignon. Asymptotic stability of the Webster-Lokshin model. In *Mathematical Theory of Networks and Systems*, MTNS, page 11, Kyoto, Japan, August 2006.

[55] D. Matignon and B. d'Andréa Novel. Décomposition modale fractionnaire de l'équation des ondes avec pertes viscothermiques. Technical Report 95 C 001, Ecole Nationale Supérieure des Télécommunications, Paris, France, 1995.

[56] D. Matignon and C. Prieur. Asymptotic stability of linear conservative systems when coupled with diffusive systems. *ESAIM Control Optim. Calc. Var.*, 11(3):487–507 (electronic), 2005.

[57] Denis Matignon and Gérard Montseny, editors. *Systèmes différentiels fractionnaires*, volume 5 of *ESAIM Proceedings*, Paris, 1998. Société de Mathématiques Appliquées et Industrielles. Modèles, méthodes & applications. [Models, methods & applications].

[58] P. McLean. Single exponential approximation of fourier transforms. *ArXiv Mathematics e-prints*, dec 2005.

[59] G. Milovanović and A. S. Cvetković. Numerical inversion of the Laplace transform. *Elec. Energ. (Facta Universitatis - Nis)*, 18(3):515–530, 2005.

[60] Gérard Montseny, Jacques Audounet, and Denis Matignon. Perfectly absorbing boundary feedback control for wave equations: a diffusive formulation. In *Mathematical and numerical aspects of wave propagation (Santiago de Compostela, 2000)*, pages 1025–1029. SIAM, Philadelphia, PA, 2000.

[61] Gérard Montseny, Jacques Audounet, and Denis Matignon. Diffusive representation for pseudo-differentially damped nonlinear systems. In *Nonlinear control in the year 2000, Vol. 2 (Paris)*, volume 259 of *Lecture Notes in Control and Inform. Sci.*, pages 163–182. Springer, London, 2001.

[62] A. Murli and M. Rizzardi. Algorithm 682: Talbot's method of the Laplace inversion problems. *ACM Trans. Math. Softw.*, 16(2):158–168, 1990.

[63] J.-D. Polack. Time domain solution of Kirchhoff's equation for sound propagation in viscothermal gases. *J. Acoustique*, 4:47–67, 1991.

[64] Mariarosaria Rizzardi. A modification of Talbot's method for the simultaneous approximation of several values of the inverse Laplace transform. *ACM Trans. Math. Software*, 21(4):347–371, 1995.

[65] R. K. Saxena. *Fractional calculus and fractional differential equations*, chapter 3, Fourth SERC School on Special functions and functions of matrix argument: recent advances and applications in stochastic processes, statistics and astrophysics, editor Mathai, A. M., pages 175–212. Publication no. 33. India, Center for Mathematical Sciences Pala Campus edition, February 2006. Lecture notes.

[66] Achim Schädle, María López-Fernández, and Christian Lubich. Fast and oblivious convolution quadrature. *SIAM J. Sci. Comput.*, 28(2):421–438 (electronic), 2006.

[67] R. A. Schapery. Approximate methods of transform inversion for viscoelastic stress analysis. In *Proc. 4th U.S. Nat. Congr. Appl. Mech. (Univ. California, Berkeley, Calif., 1962), Vol. 2*, pages 1075–1085. Amer. Soc. Mech. Engrs., New York, 1962.

[68] Thomas Schmelzer and Lloyd N. Trefethen. Computing the gamma function using contour integrals and rational approximations. *SIAM J. Numer. Anal.*, 45(2):558–571 (electronic), 2007.

[69] H.-R. Schwarz. *Numerical analysis*. John Wiley & Sons Ltd., Chichester, 1989. A comprehensive introduction, With a contribution by J. Waldvogel, Translated from the German.

[70] Dongwoo Sheen, Ian H. Sloan, and Vidar Thomée. A parallel method for time discretization of parabolic equations based on Laplace transformation and quadrature. *IMA J. Numer. Anal.*, 23(2):269–299, 2003.

[71] Frank Stenger. Approximations via Whittaker's cardinal function. *J. Approximation Theory*, 17(3):222–240, 1976.

[72] Frank Stenger. Numerical methods based on Whittaker cardinal, or sinc functions. *SIAM Rev.*, 23(2):165–224, 1981.

[73] Frank Stenger. *Numerical methods based on sinc and analytic functions*, volume 20 of *Springer Series in Computational Mathematics*. Springer-Verlag, New York, 1993.

[74] Frank Stenger. Summary of Sinc numerical methods. *J. Comput. Appl. Math.*, 121(1-2):379–420, 2000. Numerical analysis in the 20th century, Vol. I, Approximation theory.

[75] A. Talbot. The accurate numerical inversion of Laplace transforms. *J. Inst. Math. Appl.*, 23(1):97–120, 1979.

[76] L. N. Trefethen. Talbot quadratures and rational approximations. Available at http://web.comlab.ox.ac.uk/oucl/work/nick.trefethen/talbottalk.pdf, July 2006. Talk at SIAM/GAMM Applied Linear Algebra.

[77] L. N. Trefethen, J. A. C. Weideman, and T. Schmelzer. Talbot quadratures and rational approximations. *BIT*, 46(3):653–670, 2006.

[78] Lloyd N. Trefethen. Finite difference and spectral methods for ordinary and partial differential equations. available at http://web.comlab.ox.ac.uk/oucl/work/nick.trefethen/pdetext.html, 1996.

[79] Lloyd N. Trefethen. *Spectral methods in MATLAB*, volume 10 of *Software, Environments, and Tools*. Society for Industrial and Applied Mathematics (SIAM), Philadelphia, PA, 2000.

[80] P. P. Valkó and J. Abate. Comparison of sequence accelerators for the Gaver method of numerical Laplace transform inversion. *Comput. Math. Appl.*, 48(3-4):629–636, 2004.

[81] Peter P. Valkó and Joseph Abate. Numerical Laplace inversion in rheological characterization. *J. Non-Newtonian Fluid Mech.*, 116(2–3):395–406, 2004.

[82] Peter P. Valkó and Joseph Abate. Numerical inversion of 2-D Laplace transforms applied to fractional diffusion equations. *Appl. Numer. Math.*, 53(1):73–88, 2005.

[83] C. Wagschal. *Fonctions holomorphes - Equations différentielles*. Hermann, Paris, 2003. 457 pages. ISBN 2-7056-6376-2.

[84] William T. Weeks. Numerical inversion of Laplace transforms using Laguerre functions. *J. Assoc. Comput. Mach.*, 13:419–429, 1966.

[85] J. A. C. Weideman and L. N. Trefethen. Parabolic and hyperbolic contours for computing the Bromwich integral. *Math. Comp.*, 76(259):1341–1356 (electronic), 2007.

[86] J.A.C. Weideman. Optimizing Talbot's contours for the inversion of the Laplace transform. Technical Report 05/05, Oxford University Computing Laboratory, Oxford, England, 2005.

A Proof of theorem 2.1

In this section we shall give a quick proof of this interesting theorem which provides an accurate asymptotic error for the approximation of the integral of a function admitting a holomorphic extension in a strip. Indeed, the boundaries of this strip of analyticity determine this upper bound. We shall follow Henrici [40] and Schwarz [69]

Let us first recall the data:

(i) f is analytic in $\mathcal{U} = \{s \in \mathbb{C} : -c^- < \Im(s) < c^+\}$, where $c\pm \geq 0$;

(ii) $f(s) \to 0$ uniformly as $|s| \to \infty$ in $\mathcal{U}$.

(iii)
$$\int_{-\infty}^{\infty} |f(u+iv)| \mathrm{d}u \leq M^+ \qquad \forall\, 0 < v < c^+;$$

(iv)
$$\int_{-\infty}^{\infty} |f(u-iw)| \mathrm{d}u \leq M^-, \quad \forall\, 0 < w < c^-,$$

where $M^\pm > 0$.

The first step is to establish a Poisson formula. We define a periodic analytic function in this fashion:

$$T_\varepsilon(s) = \varepsilon \sum_{j=-\infty}^{\infty} f(j\varepsilon + s), \tag{41}$$

Indeed, condition (ii) ensures that this sum converges uniformly for $0 \leq s \leq \varepsilon$. Now, T_ε is ε-periodic. Hence, we define its Fourier coefficients:

$$t_k^\varepsilon = \frac{1}{\varepsilon} \int_0^\varepsilon T_\varepsilon(s) \mathrm{e}^{-\imath 2k\pi \frac{s}{\varepsilon}} \mathrm{d}s, \tag{42}$$

so that we have:

$$T_\varepsilon(s) = \sum_{k=-\infty}^{\infty} t_k^\varepsilon \mathrm{e}^{\imath 2k\pi \frac{s}{\varepsilon}}. \tag{43}$$

Injecting equation (41) in (42), and inverting summation and integration, we yield

$$t_k^\varepsilon = \sum_{j=-\infty}^{\infty} \int_0^\varepsilon f(j\varepsilon + s) \mathrm{e}^{-\imath 2k\pi \frac{s}{\varepsilon}} \mathrm{d}s = \int_{\mathbb{R}} f(u) \mathrm{e}^{-\imath 2k\pi \frac{u}{\varepsilon}} \mathrm{d}u = \hat{f}\Big(\frac{2k\pi}{\varepsilon}\Big), \tag{44}$$

wherefrom we infer

$$T_\varepsilon(s) = \sum_{k=-\infty}^{\infty} \hat{f}\Big(\frac{2k\pi}{\varepsilon}\Big) \mathrm{e}^{\imath 2k\pi \frac{s}{\varepsilon}},$$

i.e.,

$$T_\varepsilon(s) - \int_{\mathbb{R}} f(u) \mathrm{d}u = \sum_{k \neq 0} \hat{f}\Big(\frac{2k\pi}{\varepsilon}\Big) \mathrm{e}^{\imath 2k\pi \frac{s}{\varepsilon}}. \tag{45}$$

Note that the above identity is valid for all real s thanks to condition (i) according to Theorem 10.6e in Henrici [40].

The next step uses the holomorphic extension to infer the estimate from the above Poisson formula. To do so, we write the Fourier Transform (introduced in (44)) of function f:

$$\hat{f}(\xi) = \int_{-\infty}^{\infty} f(t) \mathrm{e}^{-\imath \xi t} \mathrm{d}t,$$

then perform the change of variable $t = u + \imath v$ with $0 < v < c^+$ thanks to condition (iii) to obtain:

$$\hat{f}(\xi) = \mathrm{e}^{\xi v} \int_{-\infty}^{\infty} f(u + iv) \mathrm{e}^{-\imath \xi u} \mathrm{d}u,$$

so that

$$\Big|\hat{f}\Big(\frac{2k\pi}{\varepsilon}\Big)\Big| \leq \mathrm{e}^{\frac{2k\pi}{\varepsilon} v} M^+, \quad \forall\, 0 < v < c^+.$$

In the same fashion, using the holomorphic extension in the remaining part of the strip, we yield

$$\Big|\hat{f}\Big(\frac{2k\pi}{\varepsilon}\Big)\Big| \leq \mathrm{e}^{-\frac{2k\pi}{\varepsilon} w} M^-, \quad \forall\, 0 < w < c^-.$$

Now, formula (45) can be written as follows:

$$T_\varepsilon(s) - \int_{\mathbb{R}} f(u) \mathrm{d}u = \sum_{k \in \mathbb{N}^*} \hat{f}\Big(\frac{-2k\pi}{\varepsilon}\Big) \mathrm{e}^{-\imath 2k\pi \frac{s}{\varepsilon}} + \hat{f}\Big(\frac{2k\pi}{\varepsilon}\Big) \mathrm{e}^{\imath 2k\pi \frac{s}{\varepsilon}}.$$

Therefore, using the two estimates obtained above at the limit points $v = c^+$ and $w = c^-$, we get

$$\Big|T_\varepsilon(s) - \int_{\mathbb{R}} f(u) \mathrm{d}u\Big| \leq \sum_{k \in \mathbb{N}^*} M^+ \mathrm{e}^{-\frac{2k\pi}{\varepsilon} c^+} + M^- \mathrm{e}^{-\frac{2k\pi}{\varepsilon} c^-}.$$

Computing the sums in the expression above establishes the estimate announced in the theorem.

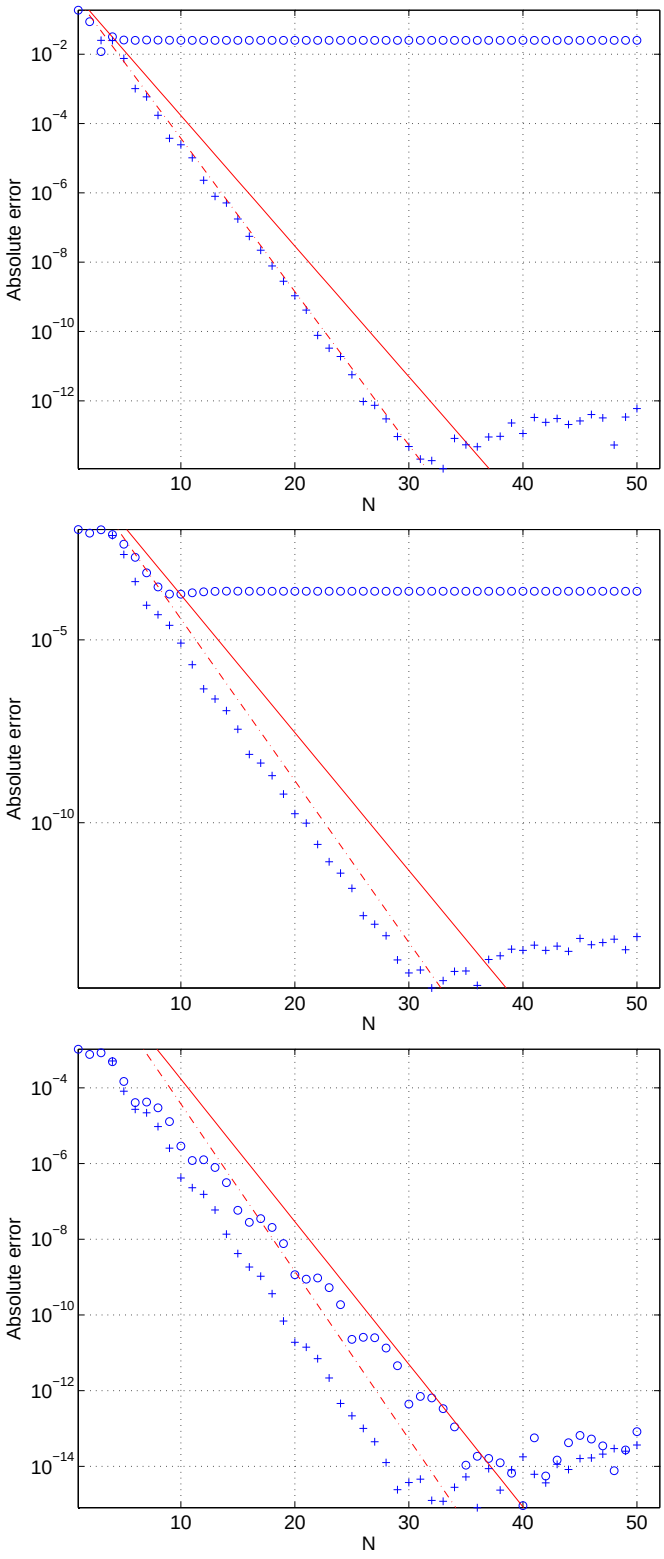

Figure 13: All three figures display the absolute error in terms of the number of nodes. The continuous (resp. dashed) line is the theoretical error for the inversion of function $\widehat{J^5}$ (resp. $\widehat{j^5}$), and the circle (resp. plus) line indicates the numerical error. The time interval's diameter is fixed $\Lambda = 10$. The first figure is initialized at $t_0 = .1$, the second at $t_0 = 1$ and the third at $t_0 = 10$.

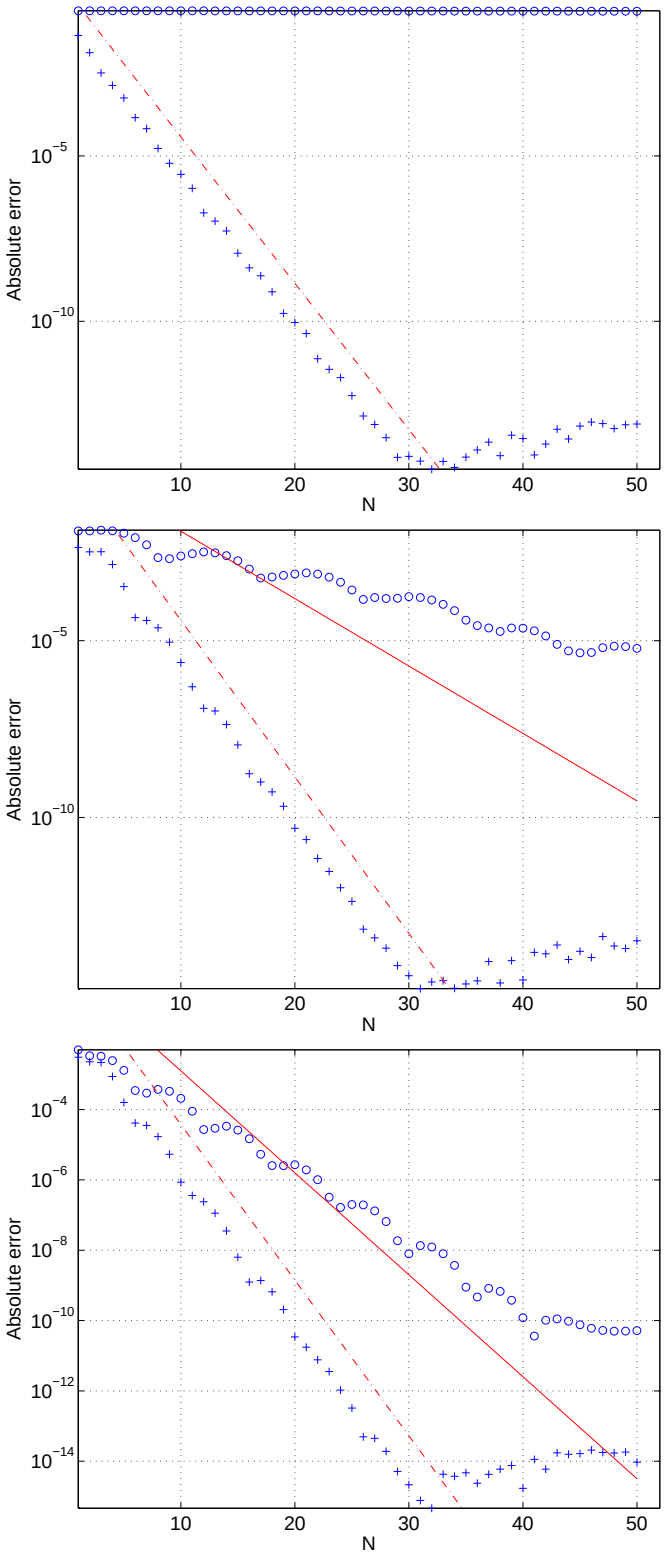

Figure 14: All three figures display the absolute error in terms of the number of nodes. The continuous (resp. dashed) line is the theoretical error for the inversion of function $\widehat{J^{\varepsilon}}$ (resp. $\widehat{j^{\varepsilon}}$), and the circle (resp. plus) line indicates the numerical error. This is computed on the time interval $[10, 100]$. The first figure displays an inversion for $\varepsilon = 0$, the second for $\varepsilon = 1$ and the last one for $\varepsilon = 2$.

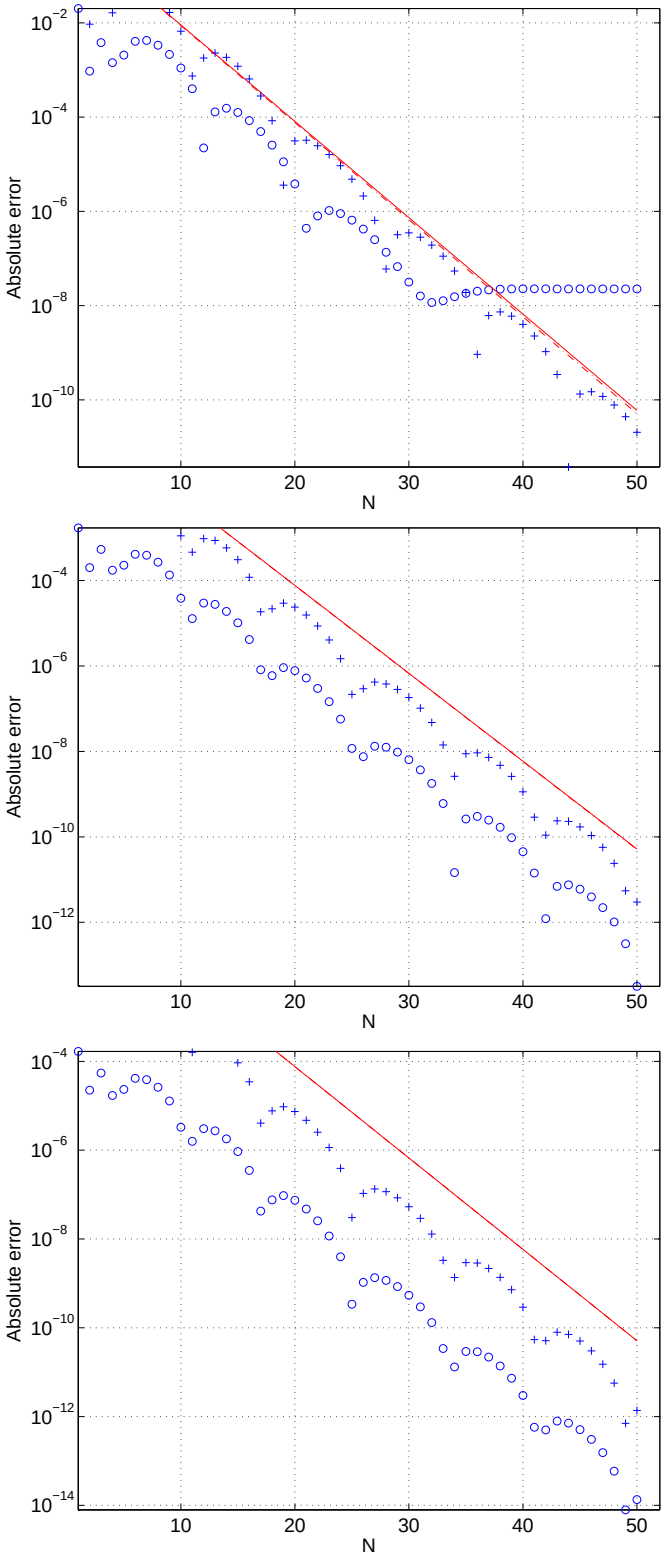

Figure 15: All three figures display the absolute error in terms of the number of nodes. The continuous line is the theoretical error for the inversion of function J_0 (resp. $j^0_\pm$), and the circle (resp. plus) line indicates the numerical error. This is computed on the time interval $[.1, 100]$. The approximations are deduced from approximations of $\widehat{J^\varepsilon}$ and $\widehat{j^\varepsilon}$ with $\varepsilon = 10^2$ on the first plot, $\varepsilon = 10^3$ on the second, and $\varepsilon = 10^4$ on the third.

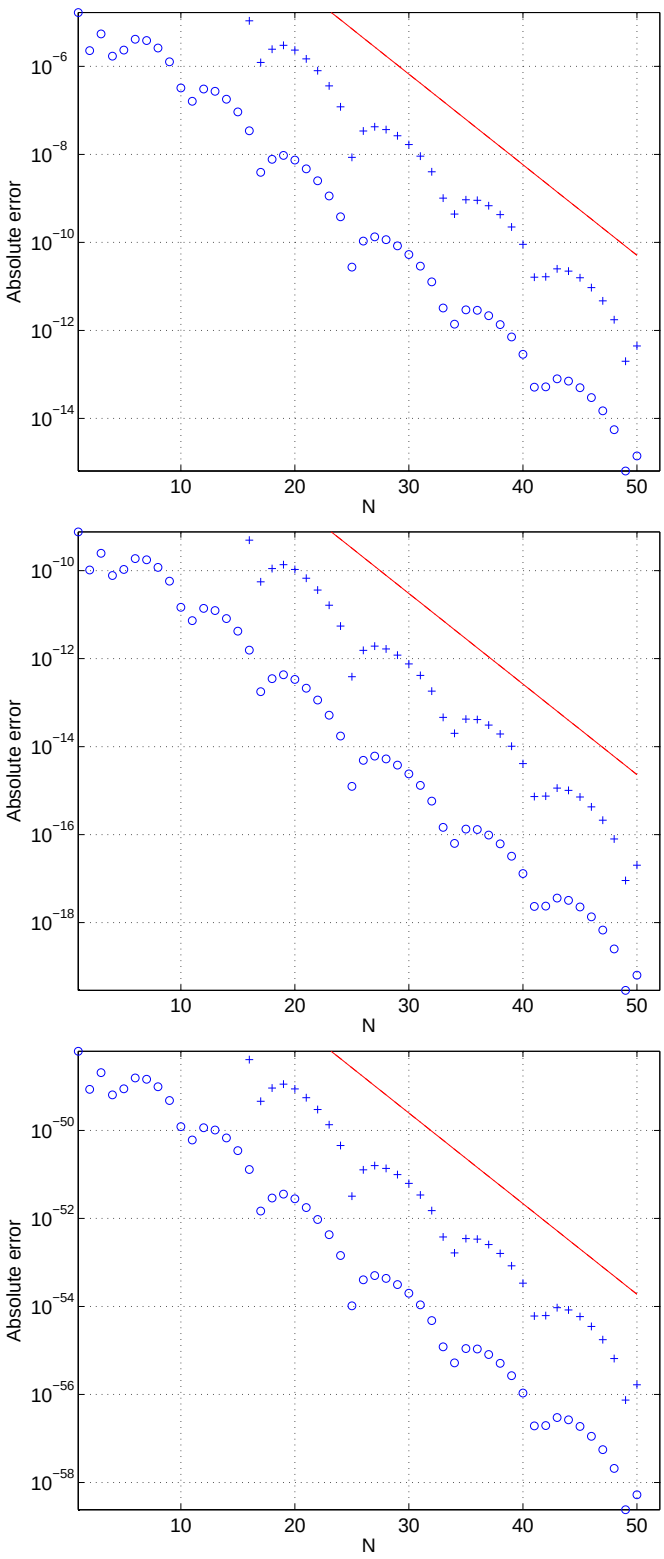

Figure 16: All three figures display the absolute error in terms of the number of nodes. The continuous line is the theoretical error for the inversion of function J_0 (resp. $j^0_\pm$), and the circle (resp. plus) line indicates the numerical error. This is computed on the time interval $[.1, 100]$. The approximations are deduced from approximations of $\widehat{J^\varepsilon}$ and $\widehat{j^\varepsilon}$ with $\varepsilon = 10^5$: on the first plot $\beta = 0$, on the second $\beta = -10^2$, and on the third $\beta = -10^3$.

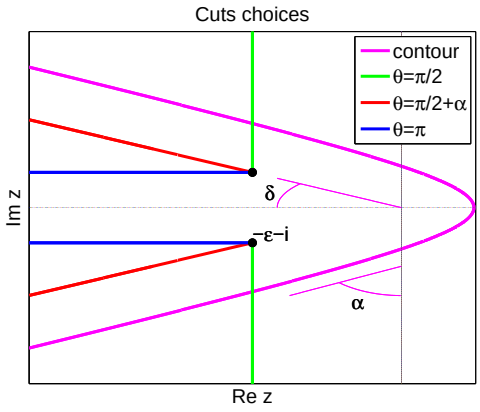

Figure 17: Different cuts: $\theta \in \left\{\frac{\pi}{2}, \frac{\pi}{2}+\alpha, \pi\right\}$.

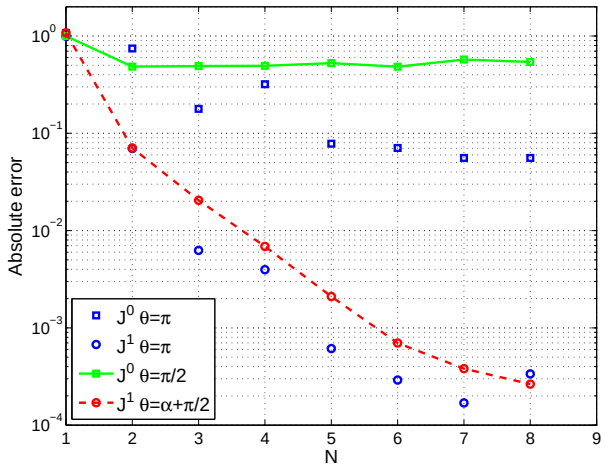

Figure 18: Approximations of J^0 and J^1 for various cuts ($\theta \approx \frac{\pi}{2}$ and $\theta = \pi$). Numerical errors.

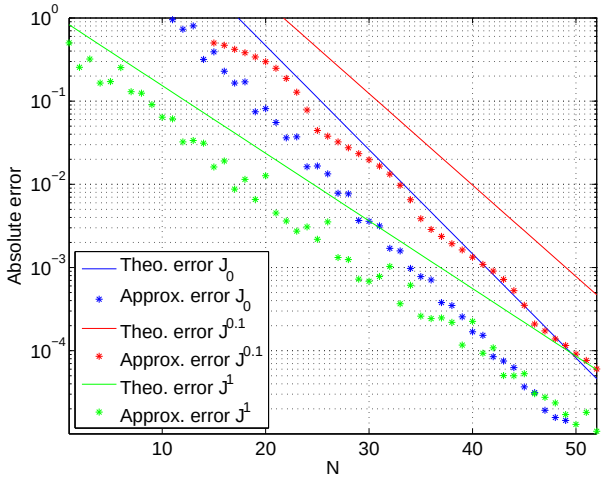

Figure 19: Different approximations of: $J_0(t),\ t \in [1,5],\ J^{.1}(t),\ t \in [.1,5],\ J^1(t),\ t \in [.1,50]$.

Dépôt légal : 2009 – 4ème trimestre
Imprimé à Télécom ParisTech – Paris
ISSN 0751-1345 ENST D (Paris) (France 1983-9999)

Télécom ParisTech

Institut TELECOM - membre de ParisTech

46, rue Barrault - 75634 Paris Cedex 13 - Tél. + 33 (0)1 45 81 77 77 - www.telecom-paristech.frfr

Département TSI